Pipeline-Seabed Interaction

Fredsøe, Jørgen

Published in:
Journal of Waterway, Port, Coastal, and Ocean Engineering

Link to article, DOI:
10.1061/(ASCE)WW.1943-5460.0000352

Publication date:
2016

Document Version
Peer reviewed version

Pipeline-Seabed Interaction (to be printed in ASCE, Waterway, Port, Coastal, and Ocean Engineering. ART NO: 10, 1061/(ASCE)ww, 1943-5460.0000352)

Jørgen Fredsoe[1]

[1]Professor in Coastal and River Eng., MEK, Techn. Univ. Denmark, bldg.403, 2800 Lyngby - Denmark. jofr@mek.dtu.dk

Abstract

A review of the existing research on the interaction between a pipeline and an erodible bed exposed to waves and/or currents is presented. The review covers three topics, i.e., scour, liquefaction and lateral stability of pipelines.

The basic mechanism that leads to scour in two-dimensional (2D) and 3D case is firstly described. The scour processes are deduced from small-scale laboratory experiments. The onset of scour from piping and the developing tunnel erosion are among the processes described. The lateral expansion of the scour hole along the pipe is described, also based primarily on small-scale laboratory experiments.. The state of the art of the mathematical/numerical modeling of the scour processes is presented. The associated self-burial of the pipe is described and compared to field observations.

In addition to scour, liquefaction may also constitute a risk for pipeline stability. The cause of liquefaction and the resulting consequence for pipeline stability in a natural environment are then discussed.

Finally, the lateral stability of pipelines placed on an erodible bed and exposed to waves is briefly described.

Introduction

Pipelines placed on an erodible seabed interact with the seabed, when exposed to sufficiently strong waves/currents. Therefore measures are usually taken to secure the structural security of the pipeline. One potential danger is the development of free spans below the pipe, which may cause the pipe to vibrate from vortex shedding. To avoid this phenomenon, pipelines are often buried in the bed, either by self-burial when this is likely to occur before any damage of the pipeline may occur, and otherwise by trenching or jetting. Even when the pipe is only partially self-buried, a benefit is that the forces on the pipeline are significantly reduced. In many areas pipelines are required to be fully buried to avoid damage by fishing gears or anchors. However pipes designed to allow lateral motion to accommodate thermal expansion should not be partially buried, which could prevent the lateral motion. A general introduction to subsea pipeline safety can be found in Palmer and King (2004).

Scour around pipelines differs from the scour around most other marine structures such as platform legs, wind turbine towers and breakwaters because of the interaction between the pipeline and the seabed. This interaction arises from the flexibility of the pipeline, which causes it to bend thus changing position during the developing scour process. The scour process continually adjusts to the changing geometry. This dynamic evolution makes the topic fascinating to deal with, but also increases the complexity of an accurate model or description of the phenomena.

When the pipe is laid on or embedded in the seabed, it changes the local flow pattern. The flow contracts and eddies are formed both up- and downstream from the pipe. The current-alone case is shown in Fig. 1. This change in flow pattern causes local increase in the sediment transport capability, which creates scour in that area. The change in flow pattern also causes a pressure difference between the up- and downstream part of the pipe, which causes seepage flow in the bed beneath the pipe, which may result in piping.

Most of the mechanisms for scour outlined below are based on small-scale lab experiments with pipe diameters varying from 5-20 cm. Many of these tests have later been modelled either by simple heuristic models or by numerical modeling tools. In recent years field data and large-scale model tests have become available.

Whether small scale experiments and numerical modeling are useful in an engineering context can be discussed: Drago et al. (2015) say "Theoretical modelling allows investigation in detail of the phenomenon occurring close to the interface and provides explanations for causes and consequences of events. But very often, owing to its complexity, it has no practical application in engineering. Usually, simplified semi-empirical interpretative models are applied. Semi-empirical models, having a strong feedback from theoretical models, try to quantify and express in formulae the outcome of experimental tests."

This statement is certainly true, since most small scale experiments have scale effects, and an idealized setup mainly uses non-cohesive sediment and an initial plane bed, and the incoming flow usually is 2D without changing direction. For this reason, most of the studies reviewed herein must be considered as a background for understanding the physics behind the scour processes.

2D Scour

63

64 ## *Onset: Piping and Scour*

65 Scour below pipelines can be split into a series of mechanisms of 2D as well as 3D in their character. These
66 mechanisms eventually lead to a certain self-burial of a pipeline originally laid on the surface of an erodible
67 seabed. Firstly, the 2D case will be evaluated, where a steady flow meets the pipeline perpendicularly, and
68 uniformity is assumed along the pipe. When not otherwise stated, the pipeline is assumed to have a
69 circular cross section with a diameter *D*, and the bed sediment is assumed to be non-cohesive.

70 When the pipe is placed *above the bed* (for instance when the pipe is unable to conform to the natural
71 bathymetry), there will generally be local erosion beneath the pipe caused by the flow contraction around
72 the pipe, causing an increase in the sediment transport capacity just beneath the pipe. This scour only is
73 significant for small initial gaps, typically less than half a diameter.

74 When the pipe is placed on or slightly embedded a certain distance *e* from the original plane bed due to its
75 submerged weight, piping may occur from the seepage flow in the sea bed below the pipe. This seepage
76 flow is caused by the pressure difference between the upstream stagnation pressure (point A in Fig. 1) and
77 the lower pressure in the leeside wake, point B in Fig. 1. In steady flow, the wake pressure is primarily
78 governed by (slightly lower than) the pressure in the separation point S (Fig. 1) because of the small
79 velocities in the wake as compared to the outer flow. In S, the pressure is low because the outside flow is
80 high (Bernoulli).

81 *Piping* failure below the pipe occurs when the hydraulic gradient i in the sediment exceeds a critical value,
82 the floatation gradient i_f, given by

83 $$i_f = (1-n)(s-1) \qquad (1)$$

where the right hand side in Eq. (1) represents the submerged weight of a unit volume of water-sediment mixture, n = porosity and s =relative density of sediment to the fluid.

The initiation of the piping begins at the downstream end (point B in Fig. 1). The piping may be facilitated by *erosion* by the up- and downstream wake system around the pipe by digging away some sediment near the pipe, Mao (1986), Chiew (1990), Sumer and Fredsoe (1991). This may contribute to the onset of piping by shortening the streamline beneath the pipe, which increases the hydraulic gradient.

The scour process initiated by piping was studied experimentally by Chiew (1990). He created a static pressure gradient using a pipe placed on/in a sandy bed in a box, divided into two equal chambers by placing a watertight partition above the pipe center. In this manner, the water levels in the two chambers could be different, and the pressure gradient below the pipe could be varied. Chiew also measured the pressure gradient around the pipe, and confirmed Eq. (1) . Sumer and Fredsoe (2001) performed similar tests using the pipe itself as the partition wall. Both studies concluded that the scour played a minor role for the onset. In the test by Sumer and Fredsoe (2001), the impact of the vortices for an embedment of *e/D*=0.064 was measured at approximately 20-25%. It is not quite clear whether this is from local scour or from fluctuations in the flow. As noted by Chiew (1990), there is another difference between static experiments and real flow. In the latter, the pressure fluctuations in the downstream vortices result in easier onset of piping.

Impact of Embedment

The onset of the scour beneath a pipeline strongly depends on the initial embedment e into the sea bed. An increase in embedment modifies the pressure gradient in the soil along the pipe periphery from A to B, (Fig. 1) in two ways; i.e. (1): the streamline in the soil becomes longer, thus reducing the gradient, and (2) the wake pressure is decreased, leading to an accompanying decrease in the gradient in the soil. The first mechanism is the most important for small embedment depths, while the latter becomes increasingly important with larger values, where the flow blocking is less, thereby decreasing the contraction flow.

Therefore, the pressure at the stagnation point S, and thereby in the wake, becomes less negative. For these reasons, there is an upper limit for the onset of scour when the pipe is embedded in the bed. In the Chiew (1990) experiments, no onset was observed when *e/D* exceeds 0.5.

Because the pressure gradient from A to B in a fully turbulent flow is proportional to the flow velocity U squared, the onset criterion can be rewritten as follows (Sumer and Fredsoe, 2001) :

$$\left[\frac{U^2}{gD(1-n)(s-1)}\right]_{cr} \geq f(e/D) \qquad (2)$$

where g = the acc. of gravity and f = a function, that depends primarily on the embedment depth. It also depends on the pipe Reynolds number and roughness, because both have impact on the wake pressure and thus influence the hydraulic gradient in the soil below the pipe. This relationship is shown in Fig. 2, where the dashed line represents the current-alone case.

In shallow waters, Chiew (1991a) additionally found the flow to change significantly with decreasing water depth at water depth below 6-8 D, which may increase the possibility for onset. This small depth-diameter ratio is most relevant in the fluvial environment.

Onset of Piping in Waves

In the wave case, the scour picture is similar to that in the current-alone case, with some modifications because the flow attack is bi-directional. The onset is governed by the same piping mechanism as explained above; however, as described by Sumer et al. (2001), the pressure gradient from A to B, Fig. 1, is a function of the Keulegan-Carpenter number KC for waves. The KC is defined as follows

$$KC = 2\pi a / D \qquad (3)$$

where a = the orbital amplitude and D = the pipe diameter. Changes in the KC cause changes in the flow pattern, e.g. the time available for piping decreases as KC decreases, because the flow changes direction

with a higher frequency when KC decreases, whereby the piping process occurs more slow in waves than in current. In addition, the pressure drop from A to B (Fig. 1) decreases as KC increases, because the downstream wake is not fully developed at small KC, and flow separation occurs further downstream on the pipe periphery than in steady current. As a result, the onset in waves for the same embedment occurs at a lower near-bed velocity in waves than in a current. This phenomenon is most pronounced at small KC (Sumer and Fredsoe, 2001).

Additionally, the potential loosening of the soil beneath the pipeline when subjected to the recurring motion associated with the orbital flow may play a role for easier onset in waves.

The waves-plus-current case. Zang et al. (2010) considered the onset of piping for the combined motion. From experiments they observed that the critical velocity for the onset of piping was slightly larger in the combined flow, and the maximum critical velocity occurs when the current velocity and the orbital motion were of the same size.

Tunnel Erosion

After piping first is initiated, it is a progressive process, i.e. the sediment moves increasingly easier. This is because the pressure gradient increases as the piping process progresses from the progressive shortening of the streamline of seepage flow (A-B in Fig. 1).

For a pipe that remains in a constant position relative to the original bed, the scour develops as tunnel scour in the 2D case from the increased flow velocity beneath the pipe. When the scoured gap develops, then the enhancement of the near-bed flow velocity decreases. The final depth is attained, when the flow velocity (or, specifically, the sediment transport rate, primary governed by the bed shear stress) below the pipe becomes the same as the undisturbed value.

154 The flow picture changes during the tunnel erosion evolution from two different causes: the change in bed
155 morphology and the changes in flow regime.
156
157 **Flow Pattern**
158 Initially, the flow velocity just beneath the pipe is higher than the undisturbed flow because of flow
159 contraction. In a steady current, the enhancement of the flow at the pipe below the axis is approximately
160 the same as that at the top, namely around 1.5 times the undisturbed incoming flow velocity, as measured
161 by Fredsoe and Hansen (1987), and similarly observed by Chiew (1991a). This flow is governed by the
162 location of the separation points of the lee wake, which are located close to the divergence of the flow, i.e.
163 nearly below and above the axis of the pipe. In this initial part of the scour process, the flow is quasi-steady
164 as scour develops. However, when the gap reaches approximately 5-10% of the pipe diameter, the leeside
165 wake experiences vortex shedding and the flow becomes highly unsteady (Sumer et al., 1988b).
166
167 **Bed Morphology**
168 The bed development for the current-alone case is shown in Fig. 3. Initially the scour occurs primarily just
169 beneath the pipe. The eroded sediment is deposited as a berm (deposition ridge) downstream. During the
170 scour development, the berm moves further downstream and levels out. The deepest part of the scour
171 hole also moves downstream. The erosion of the downstream berm is significantly facilitated by the vortex
172 shedding behind the pipe because the vortices contains high-velocity peaks (the increase has been
173 measured to be more than a factor of three), which are able to sweep away significant amounts of
174 sediment deposited in the downstream berm. This activity extends the downstream scour profile. This
175 removal of the berm makes the profile more streamlined providing less flow resistance to the flow beneath
176 the pipe, leading also to a slightly increased scour development just beneath the pipe axis. The importance
177 of the vortices has been recognized by Hulsbergen (1984), and elaborated in details by Sumer et al.
178 (1988b).

179 The final scour depth S in this 2D case is approximately 0.3-1.0 times the pipe diameter, with a high degree
180 of scatter, as shown in Fig. 4. In the figure, θ is the Shields parameter, which describes the sediment
181 mobility, quantified by the dimensionless bed shear stress as follows:
182
183 $$\theta = \tau_b /(\rho g d(s-1)) \quad (4)$$
184 where τ_b = the bed shear stress, d = the mean grain diameter and ρ = the fluid density. In Fig. 4, Re is
185 the pipe Reynolds number, defined as
186 $$\mathrm{Re} = UD/\nu \quad (5)$$
187 where ν is the kinematic viscosity of the fluid. Chiew (1991b) examined a large amount of data regarding
188 maximum scour depth beneath pipelines. Chiew' paper provides a good review of earlier experiments and
189 predictive formulae describing scour depth beneath pipelines exposed to a current. The data include pipe
190 diameters from 25 to 500-mm. He observed largest depth in the transition region from clear water to live
191 bed scour. Clear water scour defines the case where there is no general mobility of sediment on the seabed
192 from the hydrodynamic loading except very near the pipe, where the flow is enhanced. This transition
193 usually occurs at $\theta = \theta_c \simeq 0.045 - 0.050$ for sand. In the clear water case, there is no influx of sediment to
194 the scour hole. Chiew (1991b) relates the larger scour depth in this specific region to this missing supply,
195 where the measured scour actually is larger than what a number of predictive formulae suggest.
196
197 **Waves**
198 In the case of waves, the vortex shedding occurs on both sides of the pipe from the bi-directional near-bed
199 oscillatory flow. This makes the profile even flatter and more streamlined on both sides of the pipe as
200 compared to the current-alone case (Sumer and Fredsoe , 1990). The extension of the vortex street L, as
201 shown Fig. 5, primarily depends on the length of the orbital stroke or, in dimensionless form on KC , Eq. (3)

. The width of the scour hole increases also and becomes more streamlined with increasing KC . This explains the increase in scour depths with increasing KC as shown in Fig. 6. At small values of KC , the scour depth is smaller than in the current-alone case because the extension of the wake is smaller than in the current case. At larger KC (higher than approximately 50), it becomes larger than in the current-alone case because of the flattening of the profile.

Waves and Current Combined

In the combined wave-current case, there is a transition from the current-alone case, with scour depth just less than one diameter, to the wave dominated case, where the scour depth is KC -dependent. The relative strength between current- and wave-induced flow velocities is given by the parameter

$$\alpha_r = \frac{U_c}{U_c + U_m} \qquad (6)$$

where U_c = a near-bed current velocity, usually the current velocity half a diameter away from the undisturbed seabed, and U_m is the maximum orbital velocity at the bed. Drago et al. (2015) suggested, that when α_r is less than 0.8, the scour is wave-dominated, and when α_r is larger than 0.8, it is current-dominated. The value 0.8 corresponds to the limit, where the flow shifts from one-directional to bi-directional flow. Sumer and Fredsoe (1996) found a smoother and earlier transition, as shown in Fig.7. This result relates to the wake behavior around the pipe in oscillatory flow. In this flow, the lee wake vortices can be pushed back to the opposite side by the pressure gradient in absence of bi-directional flow because the wake has smaller velocities than the outside flow, and are thus easier to push back than the outer flow (Jacobsen et al. 1984).

The Time Scale

The time scale T for the tunnel erosion is a measure for how fast equilibrium develops in the scoured profile. This time scale is used to determine of the potential scour depth in a real environment, e.g. in a

single storm event. From laboratory experiments, Fredsoe et al. (1992) developed a non-dimensional time T* expressed by

$$T* = T\sqrt{g(s-1)d^3} / D^2 = 0.02\theta^{-1.7} \qquad (7)$$

According to Eq. (7), the scour process speeds up (the timescale decreases) with increasing bed shear stress θ, while no notable variation in KC is detected. In the estimate of T, an exponential variation from the initially large scour rate towards equilibrium is assumed, i.e. the estimate is an integrated approach. Dogan and Arisoy (2015) performed additional experiments, finding a variation with KC as well. In their study, the timescale is suggested to increase as KC increases. In their analysis, they distinguish between the live-bed scour and the clear-water cases suggesting different expressions for the timescale for the two different cases.

Backfill

For the current-alone case, tunnel erosion is nearly independent of the current strength, while the scour depth in oscillatory flow increases as KC increases. Therefore, an equilibrium scour profile will change its equilibrium depth when the height and/or wave period change. For example, during the end of a storm, the calmer waves may partially backfill the scoured profile because of the drop in KC. This backfill occurs at a much slower rate than the erosion because it occurs at a lower Shields number θ.

Fredsoe et al. (1992) experimentally studied the development in the scour profiles by changing the wave climate from one initial regular climate with specific values of KC and θ_i to another final one KC_f and θ_f. They found that in such transitional situations, the new equilibrium scour depth is determined by the new KC-value equal KC_f.

Time varying flow conditions

Zhang et al. (2016) performed experiments with oscillatory flow combined with a time varying current in their new large scale O-tube facility (An et al., 2013). Two types of test were done; i.e. a time-stepping flow condition and a uniformly increasing/decreasing flow condition. The oscillatory part of the motion was kept constant. In *the time-stepping approach*, a steady flow (constant flow rate) scoured in 0.24 mm sand until equilibrium was reached, where after the flow rate was changed to another either higher (causing erosion) or lower flow rate (causing backfill). Zhang et al. found similarly to Fredsoe et al. (1992) that the final scour profile is determined by the final flow conditions. Also they observed that the time scale for backfilling is much larger than the time scale for erosion. They constructed a simple time-stepping model based on knowledge on the final scour depth combined with a time-scale model. *The uniformly increasing flow conditions* were performed with a 50 mm pipe placed on 24 mm sand, and simulates the conditions during the ramp-up phase of a storm. Zhang et al. demonstrated that for this case, the developing scour can be predicted by integrating the time-stepping model, and dividing the total time period for the scour development into small time steps and calculating the scour development for each time step by the above mentioned model.

Irregular Waves

Kiziloz et al. (2013) experimentally studied the tunnel scour under irregular waves, and by comparing with regular wave tests suggested which height-period wave parameters (in the form of Significant or Root Mean Square waves) should be applied to get the best agreement between regular and irregular waves. Myrhaug and Rue (2003) performed a similar exercise numerically, based on the scour formulation by Sumer and Fredsoe (1990).

Mathematical/Numerical Modeling of the 2D Scour Development

In this section, a number of examples on the modeling of onset and evolution in the 2D scour profile are described.

Onset

Zang et al. (2009) modeled scour onset by applying a k-ω turbulence closure. They obtained the pressure coefficient distribution along the bed, which is needed to study the piping process. The calculations included different embedment depth. They also included a discussion of the changes in the pipe Reynolds number, the impact of the incoming boundary layer thickness and the water depth. They also applied the numerical model to the wave case. The seepage flow from the pressure gradient was investigated while contribution from scour near the pipe still remains to be investigated. Gao and Luo (2010) performed a similar study for the current-alone case using a numerical finite element method (FEM) for the flow above and below the pipe. Similar to Zang et al. they did not calculate the scour in the seabed either. They justified their omission by observations, which indicate that the initial scour was not near the pipe.

Tunnel erosion

Current-alone. Fredsoe and Hansen (1987) demonstrated that potential theory can predict the final gap beneath the pipe quite well. They modified the potential flow description by adding a vortex tube to ensure a more correct description of the flow beneath the pipe because the potential theory predicts much larger flow velocities beneath than above a pipe located near a bed. As explained in the previous section “tunnel erosion”, the enhancement of the flow at the bottom of the pipe is similar to that at the top (see also Chiew, 1991a). The model by Hansen and Fredsoe (1987) describes the sediment transport as bed load and followed the evolution to equilibrium, where the near-bed flow velocities beneath the pipe decrease to be equal to the far field flow velocity at the bed. Their model predicts the scour depth beneath the pipe as a function of the initial embedment, in reasonable agreement with measurements. Downstream of the pipe,

299 the evolution in the bed profile becomes too complicated for the simple model to obtain realistic profiles of
300 the scoured bed.
301 Sumer et al. (1988b) applied the discrete vortex method to focus on the impact of the downstream vortices
302 in conjunction with scour development. They showed that the peaks in the bed shear stresses caused by
303 the shed vortices were the primary agents in the lee-wake erosion.
304 Van Beek and Wind (1990) modeled the tunnel scour applying a k-ε turbulence closure. They described the
305 sediment transport applying the van Rijn (1982) sediment transport formulation. They achieved reasonable
306 agreement between predictions and the developing 2D scour profile beneath the pipe, except for the time
307 scale, which was predicted smaller than in their experiments.
308 Brørs (1999) also applied a k-ε turbulence closure, and included density effects in the momentum and
309 turbulence equations. Whether the latter is of importance is not clear from the paper. He described the
310 suspended sediment using a deposition and erosion formulation, agreeing well with the measured
311 developing scour profile in the current-alone case.
312 Li and Cheng (1999) applied a finite element solution of the potential flow to describe the scour evolution
313 with a detailed bed-load sediment transport description including bed slope effects.
314 Liang et al. (2005b) calculated scour in the clear-water case and in the live bed case, applying a detailed
315 sediment description divided into bed load and suspended load. They introduced a sand slide model to
316 smooth out numerical irregularities, agreeing well with Mao's (1986) measurement, also regarding the
317 timescale.
318 *Oscillatory flow.* Liang and Cheng (2005c) extended their current-alone studies to include the oscillatory
319 case. They investigated the phase-resolved flow and the residual (phase averaged) flow, also known as the
320 streaming. The streaming occurs because the pulsating flow beneath the pipe only is fully symmetric just
321 below the center of the pipe. Away from this location, boundary layer effects in combination with wake
322 provide asymmetry to the near-bed flow: the flow is directed away from the pipe. They demonstrated that
323 the streaming is an important feature for transporting the sediment away from the scoured profile. Their

result agrees reasonable well with the Sumer and Fredsoe (1990) experiments, but no systematic variation in scour depth with KC or sediment mobility was given.

Kazeminezhad et al. (2012) used a two-phase simulation to describe the tunnel erosion in oscillatory flow, wherein they described the formation of the scour profile and the two end-mounds around the pipe in oscillatory flow.

Fuhrman et al. (2014) also studied the tunnel erosion in oscillatory flow, using the k-ω model from the open source code OpenFOAM®. They succeeded in predicting the increase in maximum depth with increasing KC as **o**bserved from laboratory experiments, cf. Fig. 7. They demonstrated that a detailed description of the sediment transport modes is essential to calculate the shape of the scoured hole, i.e. without including the suspended sediment, the calculations predicted a bump just beneath the pipe, because the bed shear stresses opposite to the near-bed streaming pattern are directed *towards* the center of the scour hole. This bump does not appear when suspended sediment transport is included, because of the time-averaged streaming pattern in the scour hole, which is directed away from the hole.

Waves plus current. Larsen et al. (2016) applied the same modeling tool as Fuhrman et al. (2014) to investigate the scour for a wide range of combined KC and relative current strengths. Regarding the equilibrium scour depth, they obtained similar trends in the combined motion as depicted in Fig. 7. Larsen et al. also suggested an expression for the timescale in the combined flow, based on a large number of model results.

Backfilling. The backfill process, from the change in wave impact perpendicular to the pipe, was studied numerically by Fuhrman et al. (2014). They found, in agreement with the experiments, that by switching from one KC to another, the scour profile adapted to the new value of KC. Their numerical analysis also agreed well with the experiments regarding the transitional period (the time scale) for the adaptation.

Refined flow modeling. Whether even more detailed flow models provide improvements in the description of the scour is an open question. Liang and Cheng (2005a) refined the modeling by applying k-ε, k-ω and Smagorinsky´s subgrid scale (SGS) turbulence models to examine the flow around a circular pipe placed a

small distance above a plane wall. They concluded that the SGS model performed best; however, scour calculations were not included in any of the models. A more detailed description of the turbulent structures in the wake is yet to be investigated.

Refined sediment transport modeling. In the above-mentioned numerical models, different types of common sediment transport models or the Eulerian two-phase model have been applied. Because of the downstream vortex shedding with occasional peaks in the bed shear stress, a time-resolved sediment transport model is needed to describe the time scale and the final scour depths. Additionally, it is important to distinguish between the bed load (with a slope correction term) and the suspended load. In the leeside wake, next to vortex shedding, the turbulence in the wake is fluctuating; therefore, its effect on sediment transport should be incorporated in the model. Mattioli et al. (2012) performed a detailed particle image velocimetry (PIV) study of the turbulent structures in the wake around a pipeline exposed to waves. They also studied the transportation patterns of suspended sediment further away from the pipe.

Scale Effects

Small-scale experiments have limited values because the Re is usually much higher in the prototype than in the experiments. Similar to forces on pipelines, the scour patterns are sensitive to Re, pipe roughness and sediment size to pipe diameter ratio. As an example, Sumer et al. (2001) examined the change in flow regime from subcritical to supercritical regime in the flow around a pipe (corresponding to transition from laminar to turbulent boundary layer separation in the wake, Sumer and Fredsoe (2002)) by comparing the onset of scour beneath a smooth pipe and an artificially rough surface (glued .3-mm plastic particles). The limiting value for onset changes by more than 60 %, requiring much higher flow velocities for the onset of scour for a .1D burial depth. This is because, in this case, the pressure gradient from A to B drops because of the flow transition.

Zang et al. (2009) numerically studied changes in Re, but only in the sub-critical regime, where the flow changes with Re is limited.

Liang et al. (2005d) performed a numerical study of the Re dependence on tunnel scour using a k-ω model with Re-dependence in the dissipation and production terms. In their prototype model results in the supercritical range, they reported far less vortex shedding behind the pipe with corresponding smaller predicted scour depths, approximately 10-15%. Whether the vortex shedding becomes suppressed in the prototype still awaits experimental confirmation.

3D Development of the Scour Profile: Shoulders and Free Spans

Tunnel scour cannot be uniformly distributed along a pipeline, because the pipe needs seabed support. Instead, in the initial phases, scour occurs occasionally along the pipe, and then the scour holes expand along the pipe.

During this process, the pipe is supported on smaller and smaller stretches of soil, the span shoulders, as shown in Fig 8. When the span shoulders become sufficiently short, the weight of the pipe may cause a geotechnical bearing failure of the shoulder, causing larger embedment of the pipe at the shoulder. Draper et al. (2015) observed this experimentally. In their experiments, the sinking at the span shoulders occurred in small jumps in the vertical displacement, indicating a number of collapses of the span shoulders rather than a continuous bearing failure. During this process, the pipe increases its far-field embedment (defined as the local mean vertical deflection from the undisturbed seabed) as compared to the undisturbed bed by sinking down in the remaining part of the shoulders.

Sinking and sagging

Leckie et al. (2015) and Draper et al. (2015) discuss the impact of the length of the scour hole on the pipeline deformation. When the hole is long, the pipe locally sags down into the hole causing variations along the pipe, as sketched in Fig.9, left column. When, however, the lengths of the holes are shorter from the imperfection points below the pipe, the pipe sinks more uniformly.

To accurately describe the span development requires the following subtopics

- Will the scour depth beneath the pipe increase when the pipe sags down into the hole?
- What happens when the pipe touches the bed in the free span?
- How fast do the scour holes expand along the pipe?
- What will the final length of the spans and shoulders be, i.e., what are the limiting mechanisms?

Even through the scour pattern contain 3D features, much can be learned from 2D experiments and modeling. The first question in the list above can be investigated in 2D as described in the following.

Sagging Experiments

The first question in the list above was studied experimentally in a 2D setup by Fredsoe et al. (1988), who allowed a 10-cm pipe to sag in a controlled manner vertically into a developing scour hole to mimic the vertical movement of the pipe at the middle of a long span as it moves down into the scoured hole, finally touching the bed. A number of runs with different sagging velocities were performed to simulate different pipeline bending stiffness. In each individual run, the sagging velocity was constant until the pipe touched the bed. Little difference was observed between the sagging experiments and the fixed pipe tests, i.e. the depth just beneath the pipe increased by 10-20%, while the scour further downstream became slightly smaller in the sagging-pipe case. Draper et al. (2015) performed similar tests with a larger (196-mm) pipeline. Both test series mentioned above were current-alone cases. In each test, Draper et al. (2015) varied the sagging velocity with time to simulate the lateral expansion of the scour hole. These tests indicate that the scour depths increase moderately from the sagging compared to no movement of the

pipe. They also get larger scour holes beneath a slowly sagging pipe than a rapidly sagging one, suggesting that a flexible pipe sinks less than a stiffer one. The most flexible pipe studied only reached a depth of 0.58D into the bed, while the stiffest reached a depth of 1.28D into the bed. The reason for this is that the stiffer pipe reaches the bed more slowly; therefore, there is more time available to erode below the pipe. A direct comparison between Fredsoe et al. (1988) and Draper et al. (2015) is not possible because the two series of experiments use different sediment mobility parameters θ .

Both afore-mentioned studies included the scour beneath the pipe for different values of far-field embedment. It has been observed, that the scour depth below the pipe nearly doubles from around .8D for zero far field embedment, to 1.4D for an embedment of 0.9D, when the pipe sags sufficiently slowly into the scour hole. The two studies are here in line. Draper et al also confirmed (approximately) the suggested time scale for the scour development as suggested by Fredsoe et al. (1992).

Numerical Modeling: Cheng and Li (2003) modeled the scour development under a sagging pipe by calculating the Navier-Stoke (NS) equations with a Smagorinsky subgrid model. Their model predicted that the scour beneath increased with a decrease in the sagging velocity and could reach more than one pipe diameter for very small sagging velocities. Zhao and Fernando (2008) modeled the scour around a sagging pipeline with an Eulerian two-phase model to describe the sediment transport, and a k-ε model for the fluid flow. Both numerical studies agreed nicely with the measured scour profiles (Fredsoe et al., 1988).

Sinking Experiments

Draper et al. (2015) performed sinking experiments for the current-alone case and for the combined wave-current case. In the latter, the wave impact was increased gradually, to resemble a storm. In the tests, the pipe sank from the scour beneath the pipe. The scour began at the edges of the pipeline placed in a 1-m wide tunnel. When the wave impact was increased rapidly, the pipe began to move laterally because no sinking of the pipe had occurred. When the wave impact increased slowly, the scour initiated at the edges

had sufficient time to develop towards the middle of the flume, and sinking occurred from the weight of the pipe. In this case, the pipe remained laterally stable until it was completely buried.

Backfilling and Self-Burial

A scoured hole around a pipeline may later undergo sediment backfilling. One reason for this backfilling is the *touchdown* of the pipe into the scoured hole, causing the gap beneath to disappear. This changes the flow pattern because all the near pipe flow has to pass above the pipe and backfill commences, as observed experimentally (Sumer and Fredsoe, 2002) and sketched in the right column of Fig. 9. Thereby the pipe becomes (partial) self-buried. Draper et al. (2015) observed experimentally, that a flexible a pipe (with a higher sagging velocity) will self-bury less than a stiffer one, varying from 0.58D to 1.28D in their experiments. Liang et al. (2005e) modeled the backfill of the scour hole after the pipe hits the bottom of the scour hole.

Development of the Scour Holes along the Pipe

The development of the scour holes along the pipe has an impact on the sinking velocity of the pipe into the bed; i.e. when the holes spread faster, the pipe sinks faster. Several researchers have studied the migration rate without any definitive answer of the problem.

Hansen et al. (1991) performed current-alone tests, where they studied the transverse development of an initial small (artificially generated) scour hole for different initial embedment depths. The pipe was allowed to sink into the bed in the vertical direction only. They observed that the free-span development decreased with increased embedment at the shoulders. This indicates that a mechanism to stop further lateral expansion would be to decrease the length of the span shoulders such that the weight of the pipe causes geotechnical failure of the shoulders and thereby increase the embedment. Hansen et al. performed

468 experiments with two different pipe weights at the same initial embedment. They observed that the
469 heaviest pipe sank, while the lighter one did not. This is a strong indication that further sinking at the
470 shoulders is from geotechnical failure rather than to scour. Hansen et al. (1991) also investigated scour hole
471 development from an obliquely incoming current and found an increase in the propagation rate at the
472 most-exposed downstream corner, and a similar reduction in the less-exposed upstream corner.
473 Sumer and Fredsoe (1994) measured the span development in a 2-m wide current flume, where a small gap
474 between the pipe and the sidewalls ensured that the span development would begin at the sides, and
475 migrate inwards from there. In such an experiment only one shoulder appears. The pipe was allowed to
476 move freely in the vertical direction. The pipe stopped sinking at approximately 0.5-0.8 D below the initial
477 bed level. Such an experiment provides information on how large fraction along the pipe must be
478 constituted by the shoulders, while it does not give any information regarding the absolute value of the
479 shoulder or span length.
480 Cheng et al. (2009) also studied the 3D development subject to a steady current and in larger details. Just
481 as Hansen et al. (1991), they initiated the scour process by introducing a small gap in the middle of the
482 pipeline, and, again similar to Hansen et al., the pipe was partially embedded in the sand across the flume.
483 Cheng et al. observed two phases in the scour development, a higher primary rate, and a secondary slower
484 rate occurring later. Their explanation for these two different rates was that initially the pressure gradient
485 across the pipeline was large, causing strongly 3D flows in the developing scour hole, including a large
486 amplification in the near-corner bed shear stress. At later stages, the pressure gradient drops as the scour
487 hole widens, and the flow beneath the pipe becomes more 2D in its structure. For a small embedment, only
488 primary propagations were observed. Similar to Hansen et al. (1991), Cheng et al. (2009) found a decrease
489 in the scour propagation rate as the initial embedment was increased. Finally, Cheng et al. also provided
490 information on the shape of the scour hole profiles near the shoulder, i.e. they observed the slope of the
491 hole at the shoulders to be fairly constant through each test and close to the angle of natural repose.

492 Wu and Chiew (2012, 2015) performed current-alone span development experiments in the clear-water
493 regime. Like Cheng et al. (2009), they identified a rapid and a slack phase in the development. In their 2012-
494 study, they identified two driving environmental forces based on dimensional considerations, namely the
495 Shields parameter θ and the pipe Froude number F defined as follows
496
497 $$F = U / \sqrt{gD} \qquad (8)$$
498
499 Additionally, two stabilizing forces was identified; i.e. the pipeline embedment and the water depth-to
500 pipeline ratio. The dimensionless spreading velocity during the rapid development was observed to depend
501 stronger with F than with θ, but their experiments are restricted to small values of θ. Just as Cheng et al.
502 (2009), they found spreading velocity to decrease with increasing embedment, but a direct comparison
503 with the data by Cheng et al. (2009) was not possible, because Cheng et al.'s was performed with live-bed
504 conditions. Wu and Chiew (2012) observed the spreading velocity to increase with decreasing water depth
505 at water depth below 6-8.
506 Wu and Chiew (2013) performed a detailed study of the flow velocities in a span. They observed that strong
507 velocities still occurred at the shoulders, while in the middle of the span, the velocities were reduced
508 significantly. This must be associated with the strong 3D flow structure at the edge of the shoulder.
509 Wu and Chiew (2015) complemented their earlier scour measurements with measurements of the pressure
510 differential Δp between the up- and downstream part of the pipe. They measured at 4 different stations
511 spaced 20-cm between each station. They compared the temporal change in Δp with the properties of the
512 free span. They observed Δp drops at the corresponding location, where the span shoulder breaches
513 because expansion of the span. They also observed that the rapid phase is associated with a large Δp.
514 They related the initial rapid phase to the onset of scour development (piping). In the later slack phase,
515 they observed similarities to the piping phase very near the span shoulder. They measured Δp near the

span shoulders to support their statement. At the span shoulder, they measured a local enhancement of the bed shear stress next to the differential pressure between the up- and downstream side of the pipe. They concluded that both of these factors played a role in increasing the local sediment transport capacity, and are thus responsible for the propagation of the scour hole along the length of the pipe.

Waves. Cheng et al. (2014) extended their experimental investigations to include waves next to the current. They found that the scour propagation rate c decreases nearly linearly with an increase in the initial embedment depth at all wave environments studied. They related this to the reduction in the gap flow near the shoulders with increasing embedment. Further, they found c to increase as KC increases, similarly to the increase in 2D scour with KC as seen from Fig. 6. In the wave case with oblique attack, Cheng et al. (2014) found no distinction in the scour propagation rate c at the two shoulders, in contradiction to the current case, where the propagation was largest at the downstream end. This is explained by the bi-directional orbital velocities in the waves.

Conceptual Modeling of the Spreading along the Pipe

Bernetti et al. (1990) were the first to propose a simple conceptual model for the lateral spreading. Their model assumed a constant slope equal to the natural repose of the sediment, and related the scour to the rate of sediment transport. The assumption regarding the steep slope is confirmed by observations of the scour profile near the span shoulders by Cheng et al. (2009). Bernetti et al.'s model did not describe any slowdown of the spreading from pipeline caused by the embedment at the shoulders.

Hansen et al. (1991) elaborated further on a simple spreading model, in which they constructed a sediment balance at the corner of the scour hole adjacent to the span shoulder. They assumed the near-corner bed shear stress is amplified by a factor α, and that this amplification occurs at a distance βD along the pipe at the corner. β is of order O(1), while α was determined from their experiments to fit the spreading rate as best as possible using a bed-load sediment transport formulation. α decreases from approximately 2.5 for no embedment to 1.0 (no amplification) for e/D approaching 0.65. Hansen et al.´s model also included

541 the general case with obliquely incoming flow: by splitting up the incoming sediment transport into a
542 normal and parallel component, they found as later observed by Cheng et al. (2009) , that the downstream
543 corner moves faster than the upstream corner.
544 Chen and Cheng (2004) solved the 3D NS equations, including a Smagorinsky subgrid-scale model (to model
545 the eddy viscosity), and were able to calculate the complicated near-shoulder flow pattern, but without
546 experimental verification. They found bed shear stress amplifications primarily in two zones near the
547 shoulder, one just beneath the pipe and another upstream of the shoulder near the upper edge of the
548 slope.
549 In the model suggested by Cheng et al. (2009), they considered the propagation to be primarily caused by
550 tunnel erosion of the more shallow parts of the scoured hole near the corner, where the slope was
551 assumed equal to the angle of repose. The scour rate was estimated using the timescale for tunnel scour
552 suggested by Fredsoe et al. (1991), and given by Eq.6. They predicted the primary and the secondary
553 propagation rates, agreeing well with measurements in terms of the variation with different embedment
554 depths.
555 Cheng et al. (2014) finally extended their predictive model for scour propagation for the current-alone case
556 (2009) to include the wave plus current case, following the same procedure as in their 2009 paper. The 2D
557 equilibrium scour depth used in their model was adapted using a formulation by Sumer and Fredsoe (1996).
558 *Integrated approach.* Fredsoe et al. (1988) suggested in a more integrated approach that the scour hole
559 stopped developing laterally when the sinking pipe touched the bottom of the scoured hole. This very
560 heuristic model makes sense because as soon as the pipe touches the bed, backfilling might commence, as
561 sketched in Fig. 9, right column. This prevents the hole from further expansion, and the former long span is
562 transformed into two smaller free spans on each side of the touchdown point. This model therefore
563 estimates the maximum length of free spans. The model predicted proportionality between the stiffness
564 length of the pipe l_s and the maximum span length of the scoured hole. The stiffness length is the length

565 required for a pipeline to deflect one diameter from its own (submerged) weight W_s (per unit length).The
566 stiffness length is as follows
567 $$l_s \sim (128DEI / W_S)^{0.25} \quad (9)$$
568 where EI is the bending stiffness of the pipe.
569
570 **Field Measurements**
571 Leckie et al. (2015) presented 7 years field measurements along a 22.9-km long distance of a subsea
572 pipeline located on Australia's North West Shelf. They applied sonar profilers and video recordings, and
573 their study demonstrates how difficult it is to transfer knowledge based on experiments/modeling to a real
574 environment. The upper 1 m of the soil consists of drained sand along the full length of the pipeline and the
575 flow is dominated by bidirectional currents. The pipe has an outer diameter of 36-cm and the stiffness
576 length is calculated to be 44-m by applying Eq. 8. Significant self-burial of the pipe was observed. About
577 50% of the pipe was in span just after installation, and nearly all spans were shorter than 10-m. The span
578 value decreased by approximately 60% after 7 years, while the length of the spans was consistently about
579 6-m. This value corresponds to half the distance between the field joints along the pipe. No spans reach
580 more than 40 m. The large number of closely spaced spans indicates regular and frequent initiation
581 created by the joints of the pipe, which are spaced 12.2-m, c.f. Leckie et al. (2015). The long spans reach a
582 length equal to the stiffness length (44 m), which was suggested by Fredsoe et al. (1988) to be the
583 maximum value for free spans. During the seven years of observations, Leckie et al. (2015) found
584 differences to occur in the scour and self-burial pattern along different stretches along the pipeline. They
585 relate these differences to variations in soil properties and hydrodynamic impact along the pipe. They
586 found mean far-field embedment around 0.3*D* at certain stretches along of the pipe, and attaining values
587 up to 0.6*D* at other stretches. No backfilling around the pipe in the scour holes was observed. They
588 attributed this to lack of infill of sediment; i.e. the live bed scour conditions occurred less than 0.6% of the
589 total time. Regarding the along-pipe scour propagation, Leckie et al. (2015) compared the measurements

590 with the model by Cheng et al. (2009), and found the model to over-predict the propagation rate. They
591 relate this over-prediction to a wider grain size distribution curve of the soil in the field than the soil used in
592 the laboratory measurements, on which Cheng et al.'s model is based.
593
594 **Simulation of Real Storm Conditions**
595 Draper et al. (2015) simulated the environment at the North West Shelf of Australia. This area is exposed
596 to cyclones, and the wave heights can reach 10-15 m. These peak values are reached during a period of 12
597 to 36-hours. They considered the scour development in the initial stages of a storm with acceleration in the
598 near bed flow velocities. Their simulation is based on available prediction tools, and they analyze two issues
599 about the scour impact; i.e. (A) Will a pipeline increase its stability during the initial stages of a storm, and
600 (B): Will sufficient scour happen during the initial stages of a storm to ensure sufficiently stability during the
601 peak of the storm. Their considerations assume no scour is present ahead of the storm. They concluded
602 from their model simulations, that scour in the environment under consideration occurs quickly enough in
603 the initial phases of a developing storm to ensure, that significant embedment occurs during a few hours,
604 or before peak condition in the hydrodynamic forcing arrives.
605
606 **Impact of Vibrations of the Pipe on the Scour Profile**
607 When the pipe is located in a free span, it may vibrate due to waves and/or current; see e.g. Sumer et al.
608 (1989). The vibrations cause an additional pulsating flow around the pipe, which instantaneously increases
609 the bed shear stresses, thus resulting in larger ability of bed erosion. This results in an expansion of the
610 scoured bed profile. All investigations mentioned below are for the current-alone case; the wave-case still
611 needs to be studied.
612 Sumer et al. (1988a) studied experimentally the scour development in the current-alone case, where the
613 pipe only was allowed to vibrate in the vertical direction. They observed that the scour beneath became
614 wider and deeper, increasing about 30 %. The changes became especially pronounced, when the gap

beneath the pipe became large enough to allow vortex induced vibrations (VIV) to occur. These vibrations initiate larger vibration amplitudes of the pipe with associated larger scour. Gao et al. (2006) performed similar experiments and studied the impact of initial positive and negative embedment values. They observed a similar deepening of the scoured profile similar to Sumer et al. (1988a), and showed that next to the vibration amplitude also the frequency has an impact on the scour development.

Shen et al. (2000) performed scour experiments with a pipe, which was allowed to move vertically and horizontally. They found an impact from the vibrations to be slightly higher than the studies described above with a pipe with only one degree of freedom in the motion. Shen et al. found about 50 % increase in the area of the scoured profile in the dynamic case compared to the static one.

A special 3D case is investigated by Li et al. (2013), who studied scour in the transitional bend region from the vertical part to the horizontal part of a catenary riser, i.e. a vertical bend with special emphasis on scour from the oscillations of the vertical riser.

Numerical modeling. Zhao and Cheng (2010) modeled the impact of a vibrating cylinder with two degrees of freedom in motion. They applied the same modeling tool as Liang et al. (2005a,b), described above in the section “tunnel erosion”. In their numerical simulations, they provide a detailed description of the vortices developing downstream the pipe, and the changes in the vibration patterns during the scour development are analyzed. For a transverse vibrating pipe, they found numerically that the scour depth increases about 25% compared to a fixed pipe. This value increases to 30 % for a vibrating pipe with two degrees of freedom.

Other Backfilling Mechanisms

Additional to the touchdown of the pipe or changes in the wave height climate, backfilling can be caused by a turn with time in the wave-current direction: waves running more or less parallel with the pipeline alignment will backfill by infilling of moving bed load on the scoured slopes. This mechanism does not depend on any presence of a gap beneath the pipe; see Fredsoe (1978, 1979). This backfill mechanism can

result in less self-burial in the field, than suggested by laboratory experiments with perpendicular approaching wave/current.

Summary Regarding 3D Scour

The maximum length of the free spans is determined by the stiffness length of the pipe, and the observed lengths are usually shorter. A mechanism to stop the expansion of the scour hole along the pipe is the increased embedment of the pipe in the shoulders, which significantly reduces the scour below the pipe in the free span. Slow sinking rate results in a lengthening of the span, because more time is available to scour underneath. Vibrations of the pipe line will increases the length of the free spans because the scour becomes deeper. A complete model including parameters such as KC , angle of wave approach and strength/direction of a co-existing current is still lacking, but many of the elements in the process are now physically understood.

Natural Variations in Seabed Level

The natural variations in seabed level near the pipe are obviously just as important for the pipeline stability as the local scour. Migrating features can create other kinds of free span along the pipe than those described above, when the pipe is not initially buried below the lowest level of active sediment transport. An important parameter is the ratio between the stiffness length of the pipe and the radius of curvature of the bed undulation; i.e. when this ratio is small, the pipe adapts to local bed elevations, and no additional free gaps next to those created by local scour will develop. When the pipe is stiff, large gaps can develop when the sea bed curvature is large. Other important parameters are the migration velocity of the bed undulations, and the vertical variations in seabed level. These variations can be caused by several reasons:

- Bed sediments brought into suspension during storms.

- Migration of small- and medium-scale bed forms.
- Migration of large-scale bed forms.
- In nearshore areas: fluctuations in the nearshore profile.

Regarding the first item listed above, changes in the seabed level caused by entrainment or deposition of suspended sediment usually is less than a few centimeters, and therefore constitutes a minor risk. The second bullet above also constitutes a minor risk regarding small-scale bed forms, which usually are wave-generated ripples (vortex ripples), which seldom exceeds 5 to 7-cm in height. Mega ripples are the most common medium-scale bed form, which is frequent in environments with tides. The tide does not necessarily need to be very strong, because the sediment anyway can be transported by the current in combination with waves as the agitating force. Mega ripples are typically 0.5 to 2-m in height and 30 to 200-m in wave length. Typically, they migrate with a speed equal 10 to 100-m per year. The migration velocity depends strongly on their height, because high sediment waves move more slow than lower sediment waves in an otherwise identical environment. When pipelines are installed in areas with mega ripples, the pipe is usually trenched. The required trenched depth is obtained by performing statistical analysis of the trough level of the mega ripples.

Large scale bed forms mentioned in the third bullet above includes tidal banks, which are found in environments with tidal flow in combination with wind waves such as the English Channel, where they easily can reach a height more than 8 to 10-m. The propagation velocity of these banks is slow, and the slope is mild, causing the seabed level changes usually to be insignificant during a lifetime of 25 years.

Regarding the forth bullet above, the seabed variability in nearshore areas can be large. An important feature is the breaker bars, which are moving back and forth. In addition, these bars are unstable in the longshore direction because of rip currents. In these areas, the pipes nearly always are trenched below the minimum expected sea bed level.

A discussion of different spans is given in Drago et al. (2015), and includes presence of sand waves and large scale changes in sea bed bathymetry.

Other Pipe Cross Sections than the Single Circular

In this section, the 2D scour around pipelines with a cross section different from a single circular one is shortly described. Examples on such configurations are spoilers, which are installed to increase the scour and thereby facilitating the self-burial process. Also configurations such as side-by-side pipes (two in a tandem or more) or the piggy pipeline, where a smaller pipe is located on top of a larger, are described.

Spoilers

A spoiler is a small flat plate, a fin, placed vertically at the top of the pipeline. The purpose is to enhance the self-burial on the cost of a higher exposure to hydrodynamic forces. The spoiler increases the strength and extent of the downstream wake, and thereby increases the wake-related contribution to the scour, thereby facilitating the onset of scour and increase the final scour depth. Hulsbergen (1984) reports, that a spoiler can increase the self-burial depth up to 2-3 times the pipe diameter.

Chiew (1992, 1993) studied the effect of spoilers in the current-alone case and in the wave case. Spoilers with a height equal 0.25 and 0.5 times the pipe diameter were used in his experiments. These spoilers increase the scour beneath the pipe by 39 and 46% respectively. Chiew also investigated the impact of a spoiler positioned at different locations on the upstream part of the pipe. He attributed the functioning of the spoiler to two different physical mechanisms; i.e. (A): An increase in the blockage ratio of the flow, more of the incoming flow is diverted to pass beneath the pipe, and (B): An increase in the size and strength of the downstream vortex and thereby increasing the downstream lee scour.

Oner (2009) measured the flow beneath the pipe with a spoiler applying PIV, and observed that this flow hardly was increased by the implementing the spoiler.

712 *Waves.* Chiew (1993) experimentally studied the impact of a spoiler on a pipeline exposed to waves.
713 However, the pipe constituted a large fraction of the available water depth, which caused in wave
714 reflection and wave breaking. The results concerning a spoiler placed on the top therefore did not become
715 decisive for the case of a pipe located at larger water depths.

716 The impact of spoilers was studied numerically by Cheng and Chew (2003), who solved the 2D viscous NS-
717 equations, with the eddy viscosity kept constant in space. In contradiction to the later measurements by
718 Oner (2009), they predicted an increase in the flow rate in the gap between the pipe and the seabed, when
719 a spoiler is implemented.

720

721 **Tandem pipeline**

722 Two pipelines with the same diameter installed in parallel close to each other modify the scour pattern
723 beneath both pipelines. The modification depends on the spacing between the two pipelines. Zhao et al.
724 (2015) modeled the problem numerically with their (2008)-model and they compared their results with
725 experiments performed by Westerhorstmann et al. (1992). They analyzed gap ratios ranging from 0.5*D* to
726 5D and predicted for the current-alone case a slightly increased scour depth beneath the upstream pipeline
727 as compared to a single pipeline, and a much greater scour depth beneath the downstream pipe. The scour
728 attained its maximum value for a gap ratio about 2.5*D* between the two pipelines. In this case, the scour
729 beneath the downstream pipe became 50% larger than for a single pipeline. The gap ratio equal to 2.5*D*
730 coincides with the minimum distance for the vortex shedding from the upstream pipe to occur. For gap
731 ratios larger than 2.5*D*, the impact for the upstream vortex shedding on the downstream scour weakens.

732

733 **Piggyback pipeline**

A piggyback pipeline is formed by two pipelines with different diameters arranged in a bundle, with the smaller pipe located above the larger pipe, and either in direct contact with each other or with a small gap. This problem has been studied numerically by Zhao and Cheng (2008) for the current-alone case. They calculated an increase of about 40% in the scour depth for a surface mounted smaller pipeline with a diameter equal 0.2*D*, *D* being the diameter of the larger pipe. In this case, the smaller pipe functions similar to a spoiler. For a gap equal to the diameter of the smaller pipe, the scour just beneath the larger cylinder only increased by 10% as compared to no pipeline above. In the latter case, there are two vortex streets, one behind each cylinder. For smaller gaps, the two pipelines act as a single body with only one vortex street. Yang et al. (2013) also studied the flow around the piggyback exposed to waves, however without doing any scour calculations.

IMPACT OF SOIL PROPERTIES ON SCOUR

Erodibility of sandy soil depends next to the Shields parameter on the content of clay and/or silt and on the gradation of the sediment.

Sediment gradation. Armoring of the bed may occur for soil with a wide grain distribution curve, because the coarsest fraction shields the bed. This implies, that a coarser grain diameter about d_{85} shall be applied in the definition of the Shields parameter defined in Eq. (4). Dey and Singh (2008) studied the scour depth beneath a pipe placed on non-uniform sediment, and observed a large impact of the gradation. Only clear-water scour was studied, and the impact is probably also most significant in this case, where the mixing of moving sediment is minor.

Clay/Silt/sand. The content of clay or silt in combination with sand in the seabed changes the beds erosion resistance significantly by introducing cohesive properties: adding increasingly amounts of mud to sand increases the erosion resistance, with a transition occurring in the region 3-15% according to Mitchener et

al. (1996). In their study, they found the maximum resistance to erosion occurs at 30-50% content of sand. At even higher content of mud, the bed's resistance to erosion will again decrease.

Only a few studies have been made on the pipeline scour in different types of soil. Postacchini and Brocchini (2015) reported experiments with wave induced scour below a pipe in sandy soil with different concentrations of clay content. They found, that for clay content lesser than about 5%, the scour still depends on KC , and the scour decreased with increased clay content. For higher clay content, the outcome of their scour experiments became more uncertain from difficulties in establishing exactly the same initial test conditions related to compaction during reshaping of the bed. Based on their experiments, they proposed a formula for the scour depth, which next to KC also includes the concentration of clay. Additionally, Postacchini and Brocchini (2015) suggested another formula at higher clay concentrations based on data from Kumar et al. (2003) and Zhou et al. (2011).

Mohr et al. (2016) studied the time scale for erosion for a wide range of grain sizes and grain distributions, including marine sand with a clay content of 3 and 8 %. For coarser sediment, they confirmed the prediction by Eq. (7), while the time scale becomes increasingly higher for fine silt and for sand with clay content (9% finer than .2- μm). They proposed an expression for the timescale for fine sediment based on the erosion rate of the soil.

Supplementary to pipeline scour experiments, additional information on soil properties impact on scour can be transferred from the related problem of scour around a vertical cylinder. This type of structure has undergone more extensive investigations than the pipeline case, especially for the current-alone case. Dey et al. (2011) studied scour caused by waves in a sand-clay mixture around a vertical pile and found that when the proportion of clay exceeds 30%, the scour depth became the same as in clay alone. For a clay content less than 30%, the equilibrium scour depth decreases as the clay content increases. The timescale for the scour increases significantly with the clay content and with KC .

Sumer et al. (2007) considered pile scour for sand and silt with different relative density S_r of the seabed. This density is a measure for the compaction of the soil, and is given as follows

783 $$S_r = \frac{e_{v,\max} - e_v}{e_{v,\max} - e_{v,\min}} \quad (10)$$

784 in which e_v is the void ratio. Loosely dumped sand and silt may attain a relative density as low as about
785 0.35, while compacted soil reaches values up to about 0.85. The experiments by Sumer et al. (2007)
786 demonstrates that the scour increases as S_r increases, and was explained by the increased angle of friction
787 of the denser packed sediment, which makes the hole deeper for the same horizontal extent of the scour
788 hole. This is not important for the tunnel scour beneath the pipe, but may play a role at the span
789 shoulders, where the slope often approaches the angle of repose.

790 The investigation by Sumer et al. (2007) observed the *timescale* to be largest for the dense-silt case and the
791 smallest for the sand case.

792

793 Protection measures against scour

794

795 Scour can be reduced or totally avoided by installing flexible mattresses around it, either placed above or
796 beneath the pipe. The horizontal extent away from the pipe must be sufficient large, so the edge scour at
797 the outer periphery is sufficiently reduced to ensure the mats stability. Chiew (1990) experimentally
798 investigated the impact of installing an impermeable plate at the upstream side of a pipe placed on the bed
799 and exposed to a current. This plate prevents the onset of scour, because the plate lengthens the
800 streamlines of the seepage flow beneath the pipe, and thereby reduces the pressure gradient in the soil.
801 Yang et al. (2014) similarly investigated the impact of a rubber plate placed symmetrical below the pipe,
802 but only exposed to steady current.
803 On a live bed, the stability of mattresses may not be secure because of external generated morphological
804 changes. Migrating sand waves can scour around even flexible mats. In case of large degradation in the

surrounding bed area and when the mats, as is most common, are placed *above* the pipe, the impact of the protection may become negative. This negative impact happens when the mats finally hang over the pipe, and thereby enhances the scour by sweeping away sediment, when the mats move back and forth by waves and current. Problems similar to these are also encountered near the pipeline inlet to an offshore platform. In this case, the platform itself may create a depression in the bed area from local scour around the platform.

The most flexible scour protection is a falling apron consisting of wide graded material. This protection can withstand moderate bed level changes without serious damage. Flexible mats may also work as protection against scour, if they are placed properly *below* the pipe.

Liquefaction

Non-cohesive soil in the seabed exposed to waves may undergo liquefaction, where the soil-water mixture is transformed into a liquid. When liquefaction occurs, pipelines originally placed on the seabed may sink, when their submerged density is higher than the liquefied soil density. Buried pipelines may similarly float to the bed surface, when their submerged density is smaller than that of the surrounding liquefied soil.

Cohesive soil may liquefy in the way that it can lose its shear strength during cyclic loading (strain softening, cyclic degradation as described by e.g. Vucetic (1991)). In the following description, focus is primarily directed to non-cohesive material.

Usually liquefaction caused by earthquake is the major cause for liquefaction of soil because its large amplitude in the oscillation and higher frequency (earthquake: O(1sec), waves: O(10 sec)). However, also waves can cause liquefaction as detailed in two recent books by Jeng (2013) and Sumer (2014). In the wave case, the cyclic variation in shear stresses in the soil is caused by the pressure variation along the seabed

828 from the migrating surface waves (positive pressure under the crest where the water depth is large and
829 negative pressure under the trough). These pressure variations induce shear stresses in the soil, when the
830 waves propagates as shown in Yamamoto (1981) and Madsen (1978), who both provide analytical solutions
831 for the induced shear stresses in the soil.

832 Sawaragi and Deguchi (1992) showed that in the soil, the wave-induced bed shear stress has negligible
833 impact on soil shear stresses as compared to the stresses induced by the bed pressure variations from the
834 waves.

835 Liquefaction of the seabed caused by waves can occur in two different ways: beneath the wave trough, the
836 seepage flow is upward directed, because the small seabed pressure. This loosens the soil and eventually
837 causes the soil to be liquefied. Since this kind of liquefaction only has a short duration during passage of the
838 wave trough, this is called *instantaneous liquefaction*.

839 The other mechanism is related to loosely deposited sediment, which can be compacted by the waves, and
840 thus create of an excess pore pressure in the bed soil. During the compaction phase, this pressure may be
841 sufficiently large for a period of time, causing the effective grain stresses to disappear, and liquefying the
842 soil. This type of liquefaction is called *residual liquefaction.*

843

844 *Instantaneous Liquefaction*

845

846 Instantaneous liquefaction is the process, where a column of soil can be lifted by a pressure lift force. This
847 force is caused by the difference between the wave induced excess pressure in the soil at a depth z below
848 the sea bed surface and the pressure at the seabed at the same location. When this difference becomes

849 larger than the overburden pressure of the soil-fluid mixture, the soil will move vertically as a block. The
850 overburden weight W above a level z below the sea bed is as follows

851 $$W = \rho(s-1)gz(1-n) \qquad (11)$$

852 In Eq. (11), n is the initial porosity of the soil. The upward directed hydraulic gradient i in the soil below
853 the wave trough must exceed $W/(\rho g)$ to obtain instantaneous liquefactions. In a discussion of the paper
854 by Moshagen and Tørum (1975), Prevost et al. (1975) demonstrated, that hydraulic gradient usually is too
855 small to create liquefaction, even under large waves.

856 *Impact of gas.* When the soil contains gas, the vertical pressure gradient just beneath the seabed surface
857 increases, because wave-induced pressure dampens faster from the sea bed. This dampening is caused by
858 the higher compressibility of gas compared to fluid (Tørum , 2007). The gas (most common Hydrogen
859 Sulphid) can stem from deterioration of organic material, and there is nearly always a small fraction of gas
860 as a part of the fluid in the seabed, but it is difficult to measure, see e.g. Sandven (2007). Tørum (2007)
861 suggests that 3% gas content may be enough to introduce liquefaction at the seabed. However, when the
862 gradient is steep, the liquefied layer will correspondingly be thin, and therefore the impact on vertical
863 motion of a pipeline may be negligible.

864 *Impact on pipe movement.* The pipe can adjust its position vertically as well as horizontally, when the
865 surrounding soil is liquefied and the pipeline specific gravity is different from that of the liquefied soil.
866 However, in a real environment, the instantaneous liquefaction must occur simultaneous a minimum
867 distance along the pipe to allow movement. This distance must constitute at least a considerable fraction of
868 the stiffness length of the pipe to obtain movement of the pipe. This condition requires the waves to
869 approach the pipe nearly perpendicularly and have a strong 2D-feauture; i.e. long wave fronts.

870

Residual Liquefaction

Residual liquefaction is the process, where loosely deposited fine sediment is moved internally back and forth by shear stresses and obtains a denser, compacted grain skeleton. When this sediment is loaded for the first time (named “virgin loading” by e.g.de Groot et al (2006)), the individual grains can easily rock or even pass over the underlying grains. In average they obtain a denser packing, sometimes after a transient even looser packing (dilatation) during the passage of one grain above the other. This process is well-described by De Grooth et al. (2006). The internal displacement of the grains is primarily caused by shear stresses, while an overall increase or decrease in normal stresses (pressure) only causes compression. Sawicki (2014) argues that the *gradient* in normal stresses also contributes to internal displacement.

The compaction process leaves empty space, and implies a reduction in the effective grain stresses. Therefore, redistribution between soil and fluid stresses occurs; i.e. at this stage the fluid pressure carries a higher fraction of the overburden pressure W originating from the sediment-water mixture above, while the effective stresses between the grains reduce correspondingly, and thereby increases the excess pressure p^+ in the fluid. This pressure acts on the fluid, and squeezes the excess water from the soil-fluid mixture into the fluid above the seabed. Thereby the excess pressure is relieved. When this relief does not occur fast enough, the excess pressure p^+ at a depth z might build up to a level that exceeds W and the soil-fluid mixture becomes liquefied above this depth.

The conditions for the soil to liquefy therefore depend on the strength of the cyclic shear stress, the number of waves, the permeability of the soil and the initial compaction ability of the soil skeleton before heavy wave impact. For cohesion-less soil the latter is most often characterized by its relative density.

Therefore, the requirement for liquefaction is

- Sufficiently large waves to ensure that a high value of the excess pressure p^+ is obtained.
- Low permeability soils, causing p^+ not to be relieved sufficiently quickly; i.e. the sediment must not be too coarse because coarse sediment has a large permeability.
- Loosely deposited sediment, where the grain skeleton can be consolidated in the virgin load phase.

Fig. 10 shows a typical recording of the variation in p^+ at four different vertical levels in a flume test performed by Sumer et al. (2006c), where loosely silt liquefies by propagating waves. The recording shows the typical features of the cycle; i.e. initially, the pressure build-up begins quite similarly at all measured depths in the soil and this build-up occurs during the first minute after the waves are switched on. This time corresponds to the time the grains need to obtain a denser configuration. The increase in p^+ ceases, as liquefaction evolves at the different z-values.

The liquefaction begins initially at the surface of the bed, where least overpressure is required to carry the overburden weight W, which increases as the distance z from the bed increases, c.f. Eq. (11). From the bed surface the liquefaction penetrates downward until the depth is reached, where p^+ becomes smaller than W.

The second stage is a decrease in p^+ because of an outflow of the excess water in the bed. This outflow is created by the upward hydraulic gradient in p^+, and begins at the transition from the solid to the liquefied bed (the solidification line.) When the fluid escapes, the grains in the liquefied mixture begins to settle on the solidification line, and now in a more compact manner than in the former loose phase. The compaction is ensured by the oscillatory shear stress variation by the waves, and as a result the solidification moves upward, causing a denser compacted bed at the end, as observed in laboratory experiments, Sumer et al. (2006a). Sawicki (2014) discusses the re-solidification, and states that earlier liquefaction is erased, because the soil once more will be loosely deposited, causing the virgin state to be reestablished. This is not in line with laboratory investigations like Sumer et al. (2006a), however it may occur under

916 circumstances like a sudden decrease in the environmental impact. If pre-consolidation does not exist from
917 earlier storm events, the potential liquefaction risk increases considerably.

918 *Impact of the pipe on liquefaction.* The presence of the pipe itself in the soil will change the liquefaction
919 patterns compared to those developing in homogeneous soil: Sumer et al. (2006b) observed a faster
920 buildup of the excess pressure, when the pipe is present. Initially the liquefaction was observed to occur
921 just beneath the pipe, while the impact of the presence of the pipe at the top of this pipe was negligible.
922 This is in accordance with the numerical modelling results by Dunn et al. (2006).

923 *Experiments.* Laboratory experiments can be performed in a wave flume with real waves or by centrifuge
924 tests. The records shown in Fig. 10 are based on small scale laboratory wave flume experiments with 10 to
925 20-cm high waves. Because the stress-strain relationship of the soil depends on the stress level, many
926 liquefaction experiments are performed by centrifuge tests to obtain prototype stress levels in the soil; see
927 e.g. Sassa and Sekuchi (1999) and Miyamoto et al. (2004). Introducing dimensionless parameters, Sumer
928 (2014) obtained a good agreement between the two types of tests regarding the pressure built up.

929

930 *Behavior of a Pipeline in a Liquefied Bed*

931

932 A change in the pipe position primarily occurs in residual liquefied soil, which in contrast to instantaneous
933 liquefied soil includes a larger area of the seabed simultaneously.

934 Sumer et al. (1999) considered the 2D case in the laboratory; i.e. a 4 cm pipe was placed with its center 5-
935 cm below a seabed, which consisted of 0.045 mm silt. The seabed was exposed to waves and became
936 liquefied. The pipe was found to adjust its vertical position in the liquefied flow depending on the ratio of
937 pipe specific gravity ρ_p compared to the specific gravity of the sediment-fluid mixture of liquefied soil ρ_l :

when ρ_p is higher than ρ_l, the pipe obviously will sink, and adjust its vertical position to that level, where the two densities become the same. ρ_l usually increases as the distance z from the bed increases, because the grains in the liquefied soil settle, see e.g. Sumer et al. (2006c), Typical average values of ρ_l is 1.8-1.9 ρ, which provides an estimate for whether the pipe will sink or float.

Teh et al. (2003) similarly tested a 7.5 cm pipe in 0.033 mm soil. The specific gravity of the pipe varied from 1.1 to 2.1. They observed that for specific gravities more than 1.8, the pipe sank in the liquefied soil. Teh et al. (2003) divided the pipeline behavior into three different modes; i.e. (A): A light slow sinking pipe, where the excess pore pressure in combination with the liquefied soil acts as a buoyancy force on the pipe. (B): A light pipe in combination with more permeable soil; i.e. when the excess pore pressure dissipates quickly, the pipe stops sinking before the pipe has attained its equilibrium position. This is because the solidification line in the meantime has moved upward, and prevents further sinking. (C): The pipe is heavy (fast sinking), causing it to sink before the excess pressure disappears. In this case the pipe simply reaches the lowest level of the solidification curve. Teh et al. (2006) developed a simple analytical model for the sinking velocity of the pipe and for the rising velocity of the solidification curve.

Residual Liquefaction in a Natural Environment

Similar to scour, liquefaction also needs time to develop, and similar to scour, the question occurs regarding liquefaction about what happens during the rise and fall of a storm. Can the initial phases of the storm create liquefaction followed by solidification, before the peak conditions occur; i.e. what is the timescale for the whole liquefaction process compared to the acceleration of the storm? When the bed becomes liquefied during a storm, the next question is whether in the final part of the process, the compaction will be completed before the hydrodynamic impact has ceased. The timescale for compaction

960 strongly depends on the settling velocity of the fine sediment, which can be small because of the large
961 concentrations of sediment in the liquefied soil; i.e. “hindered settling”.

962 When the compaction process is fully completed, liquefaction should not be possible to occur a second
963 time, when the bed once more is exposed to a storm with same strength and duration, because the soil is
964 no longer in its virgin stage, but pre-consolidated. Whether an even heavier storm in this case will give rise
965 to liquefaction is a little bit open; i.e. will the upper compacted layer act as a shield for a lower less
966 compacted layer?

967 When the compaction process has not been completed fully up to the surface of the seabed before the
968 storm has ceased, the sediment in the upper layer will settle loosely in the bed, and can easily be liquefied
969 again. However, the lower layers can be compacted, because the compaction process begins from below.
970 This compacted layer may act as a shield for additional penetration of the liquefaction into the bed, but
971 experimental evidence for this situation has not been studied experimentally yet.

972

973 **Impact of Fines in the Soil**

974 Loose sand often has a content of finer material of silt or clay in the pores. Kirca et al. (2014) studied the
975 influence of clay content on the liquefaction risk. The presence of clay in sand/silt reduces the permeability
976 of the soil, and thereby allows the excess pressure to rise to a higher value, before the drain of excess
977 water begins to relieve the excess pressure. Even coarser fractions of sediment such as fine and medium
978 sand increase their risk of being liquefied, when the clay content is sufficiently high. In their experimental
979 study, Kirca et al. (2014) observed, that at least 10% clay content was necessary to obtain liquefaction for
980 0.4 mm sand. In addition, they observed in their experiments with silt, that when the clay content exceeds
981 about 30 %, the clay-silt matrix changes its physical properties; i.e. the matrix behaves as high plasticity

clayey silt, which will not allow the coarser grains to rearrange under the cyclic shear strains. Liu and Jeng (2015) performed similar experiments and found the same trends.

Measures against Liquefaction

A risky area for being liquefied is the backfilled cover of a trenched pipe, where the soil can be loosely deposited. This cover is one of the most vulnerable locations for possible liquefaction until it has been compacted by waves, most likely through a liquefaction process. The risk of liquefaction of a backfilled trench can be reduced by adding layers of permeable material (coarse sand, pebbles, and stones) above the trench. These additional layers imply that the excess pressure must overcome a larger weight W to liquefy the soil, and additionally the coarse layers remove the risk of liquefaction in these upper layers. The impact of adding a cover layer of armor stones on top of liquefiable sediment was studied by Sumer et al. (2010).

Mathematical/Numerical Modeling

The cyclic variation in shear stresses and pressure and the resulting build-up of the excess pressure caused by compaction can be modeled using the following four sub-elements:

- A shear-strain relation for the soil.
- Knowledge of the compressibility of the fluid and the soil skeleton.
- A relationship for the consolidation describing the pore volume reduction by the cyclic imposed shear and pressure.

- A flow resistance law (such as the Darcy law) to describe the seepage flow as a function of the hydraulic gradient.

The wave-induced cyclic soil stresses have been calculated by numerous researchers, and a comprehensive review is given by Jeng (2003). This review describes next to the classical solution of seepage flow in a porous incompressible and non-deformable bed (see e.g. Sleath (1970)) also a number of numerical/analytical studies, where the fluid and/or the grain skeleton are compressible. Most studies are based on Biot's (1941) consolidation model.

Instantaneous liquefaction. Moshagen and Tørum (1975) treated the wave induced seepage flow by including the compressibility of the fluid phase, while Yamamoto (1977) and Madsen (1978) also included the compressibility of the soil in their analysis to calculate pressure and shear stresses.

Residual liquefaction. The consolidation is usually considered as a plastic deformation. Examples of such solutions are given by Rahman et al. (1977) and McDougal et al. (1978). They introduce a pore water pressure generation term, which depends on the magnitude of shear stress, number of waves, soil type and relative density of the soil.

A large number of later studies on anisotropy, limited soil depths etc. are described by Jeng (2013) and Sumer (2014).

Does Loosely Deposited Sediment Exist in the Seabed

As discussed above, soil exposed to waves usually consolidates, however with some reservations regarding the timescales for the liquefaction process. In addition to a recent backfilled cover of a trenched pipe, other risky locations can be areas where compacted seabed soil is loosened. This occurs when the seabed

becomes stirred up by natural variations in the seabed as mentioned earlier. As an example, the sand passing the crest of migrating sand waves and deposited on the sand wave front is loosely deposited.

Lateral Stability of a Pipeline on an Erodible Bed

Scour around a pipeline changes its stability against lateral motion. However, nearly no investigations have been performed which include the impact of scour on the lateral movement of a pipe. The most common case studied by geotechnical scientists is the impact of passive soil resistance on a pipe from the slight embedment. A pipe placed on a soil surface usually will experience a slight embedment because the submerged weight and also because the installation procedure. When embedded and exposed to hydrodynamic forces, the pipe experiences resistance against lateral motion from two contributions; i.e. a frictional component and a passive resistance component from the soil. This problem can be investigated experimentally by moving the pipe back and forth on a saturated soil bed in a controlled manner.

Based on experiments with a sandy bed, Gao et al. (2007) describes the behavior of a slightly embedded pipe, which loses its lateral stability as a result of continuously increasing action by current or waves. In the *current-alone* case, the pipe initially pushes the nearby soil ahead with an associated slight lateral pipe displacement, until it at a certain time loses its stability and breaks out with a resulting large displacement in the current direction. In the *wave case,* the pipe initially rocks back and forth with the wave period and a very small amplitude. Very soon, the amplitude of the pipe-motion increases to significantly larger horizontal displacements, and this motion creates a berm on each side of the pipe by pushing the sediment. Regarding the current-alone case, Gao et al. (2011) found experimentally (using a mechanical-actuator simulation) that the distance by which the pipe moved before breakout decreased with increasing initial embedment.

1046 Wagner et al. (1989) performed a number of tests with a rig, which moved pipes with diameters equal 0.1-
1047 m and 0.5-m back and forth over a sandy and clayey bed. Because only air and no fluid was present above
1048 the sediment bed, the scour and seepage flow are not present in the experiment. The properties of the
1049 sand range from loose silty sand to loose and dense medium to coarse sand. The pipes were moved in a
1050 controlled manner vertically and horizontally. Wagner et al. found that in the sandy-bed case, the largest
1051 increase in passive soil resistance occurred in the case of loose medium sand. This result is linked to the
1052 larger penetration of the pipe in loose than in dense sand. They suggested a formula for the total lateral
1053 soil resistance F_H in a sandy bed given by the sum of a sliding resistance component and a passive soil
1054 resistance component

1055 $$F_H = \mu\left(W_S - F_L\right) + \beta\rho g(s-1)A \qquad (12)$$

1056 Here, W_S is the submerged weight of the pipe per unit length, F_L is the hydrodynamic lift force, μ is the
1057 sliding resistance coefficient (which they put equal 0.60), A is half the soil cross-sectional area displaced by
1058 the pipe caused by penetration and oscillations, and β is an empirical dimensionless coefficient, which was
1059 measured to vary from 38 for loose sand to 79 for dense sand. With this model, they obtained nice
1060 agreement with measured and calculated lateral pipe motion.
1061 Wagner et al. (1989) also tested a pipe placed on a *clayey* bed, and in this case the contribution from the
1062 lateral soil pressure relative to the total soil resistance was measured to be larger compared to the sandy-
1063 bed case. This increase is because the pipe sinks more in clay than in sand. Wagner et al. finally studied the
1064 impact of consolidation of the clay: in the first number of cycles, the consolidation increases the soil
1065 resistance, but this effect disappears after a few cycles even at a few small amplitude oscillations. For the
1066 clay-case, they proposed a formula similar to Eq. (12), but the last right side term was changed to $\beta cA / D$
1067 , where c is the remolded undrained shear strength for clay. In the clay-case, β depends on pipe
1068 displacement and lateral load history.

1069 Hale et al. (1991) concluded that Wagner et al.'s model is conservative, when compared to the pipe/soil
1070 tests on which they are based.
1071 Gao et al. (2002) studied the soil resistance in the more realistic case, where fluid is present above the bed.
1072 The experiments were performed in a U-tube, and the pipe was moved back and forth by the fluid forces in
1073 two modes; i.e. with or without rolling (anti-rolling). To obtain sufficient information on the interaction
1074 between the developing scour and ploughing from the pipe's lateral motion, they performed a large
1075 number of experiments with different Shields parameters and different amplitudes and frequencies in the
1076 lateral pipeline motion. Gao et al. (2002) also performed a number of combinations of lateral motion and
1077 initial embedment of the pipe, while the variation in the Shields parameter was limited. Therefore the
1078 importance of scour on the initial lateral motion was not fully clarified. However, by increasing the
1079 oscillatory fluid action gradually, they observed that onset of scour developed before the pipe began to
1080 rock. The breakout from its original position occurred as the last stage of the pipeline instability. For certain
1081 near-bed flow strength, they observed the pipe to be more unstable in waves than in a steady current.
1082 Anti-rolling pipes were found to be much more stable than freely laid rolling pipelines. Gao et al. (2007)
1083 provides alternative expressions to those by Wagner et al. (1989) for the lateral stability in waves and in
1084 current for the sandy-bed case. They suggested the stability to be as follows

1085 $$F = \alpha + \beta G \qquad (13)$$

1086 in which F is the pipe Froude number and G is the dimensionless submerged weight of the pipe

1087 $$G = W_S / (\rho(s-1)D^2) \qquad (14)$$

1088 The two constants in Eq. (13) depend on the soil and whether the pipe is exposed to current or waves: α is
1089 0.1 and β is 0.42 for medium sand combined with a current. For fine sand, β decreases to 0.2. In the case
1090 of waves in combination with medium sand, α decreases to 0.05, while β maintains the value 0.4.
1091 The impact of *pipe roughness* was investigated by Gao et al. (2011). Initially a rough pipe has a smaller
1092 embedment than a similar smooth pipe, but the final maximum settlement in the breakout process is larger
1093 for the rough pipe case. The impact of the initial sand bed *slope* for the pipes lateral stability in waves was

studied by Gao et al. (2012). They found the soil resistance increases most regarding the downslope instability, and the lateral-soil-resistance coefficient is larger for the up- and down-slope case compared to the corresponding horizontal seabed case.

Large lateral motion. White and Cheuk (2008) studied the soil-pipe interaction over soft cohesive soil (kaolin clay), where the lateral motion was about 10-20 times the pipe diameter, to allow the pipe freely to buckle laterally in a controlled manner caused by thermal expansion. In this case, self-burial is unwanted, and a detailed description is given of the berm development around the pipe, when the pipe is moving back and forth and ploughing the bed. The importance of these berms is that when they are created by moderate wave action, they can increase the passive soil resistance at even higher waves, than those which formed the berms. This increase will restrict the possibility for larger lateral motion. White and Cheuk (2008) provided a heuristic model for the large lateral motion of the pipe based on a simple kinematic hardening model for the soil.

Modeling

The modeling of the pipeline soil resistance is primary performed applying a geotechnical perspective without including possible scour from the flow. The models are heuristic in their character. The clayey soil behavior is complex and only behaves elastic for very small deformations. At larger deflections, the constitutive equations include plastic deformation within the yield surface. The changes in strength can decrease the soil resistance with time from softening; i.e. cyclic degradation of clay as described e.g.by Vucetic and Droby (1991). Clay as well as non-cohesive soil can also undergo hardening from consolidation and compaction as described e.g. by Elgamal et al (2003).

Zhang et al. (2002) modeled the stability of a pipe placed on an elastic-plastic medium, where the bed deformation is based on a kinematic hardening model, such that the pre-loading history is memorized. They did not split the flow resistance into two terms as was done by Wagner et al. (1989), but introduced an integrated model, where induced incremental displacement tis linked to the incremental load. The

hardening was linked to the vertical plastic displacement and was calibrated with existing centrifuge test to obtain a valid full scale model. It has a smooth transition from the elastic state at small loads to the plastic state at the yield. Tian et al. (2010) observed that the hardening law deviates from the centrifuge test for relatively small pipeline lateral displacements less than about half the pipe diameter. Tian et al. attribute this discrepancy to the missing presence of the berm in previous models, and they included this in the model. However, no scour was included.

Liquefaction Caused by Pipe Motion

The movement of the pipe on the seafloor can create instantaneous liquefaction as described by Foray et al. (2006). They observed a strong increase in the excess pore pressure at the pipe-soil interface around a cyclically loaded pipeline. The increase is sufficiently large to create instantaneous liquefaction in a soil band close to the pipe wall. Because a strong negative pore pressure occurred when inverting the loading direction, there was no general residual liquefaction observed in the experiments by Foray et al. (2006). The instantaneous liquefaction caused an increased penetration of the pipe into the seabed. This increase resulted in a larger lateral resistance. The increased densification of the soil and the negative pore pressure on the downstream part of the pipe also contributed to a larger soil resistance.

Pipe Behavior on a Liquefied Bed

The special case, in which the bed becomes liquefied but without any scour around the pipe has been studied by Teh et al. (2003) in a wave flume with silt in the bed. They performed their experiments with low Shields numbers to avoid the scour. They studied the behavior of two pipes, both of which were heavier than the surrounding fluid-soil mixture, but one was significant lighter than the other. They identified two different types of behavior; i.e. the light pipeline became unstable before the bed became liquefied and formed a small trench by rocking before the soil became liquefied. On the contrary the heavy pipe caused the bed to liquefy before the pipe began to rock. Similar to Sumer et al. (1999), Teh et al. observed that the

heavy pipeline sank to a specific level in the liquefied soil, depending on soil parameters and the specific gravity of the pipe. The final embedment of the heavy pipeline was influenced by the initial embedment depth of the pipe, while it was not the case for the light pipeline.

Impact of Scour

The impact of scour has only been included in very few experimental tests; i.e. those by Gao et al. (2002). Because the deposition berms at the downstream side (current alone) or both sides (waves) are formed by soil pushed by the pipe and therefore recently deposited, the berms are easy to erode. Therefore reshaping of these berms caused by flow around the pipe is most likely to occur.

Conclusion and Future Research Needs

Pipeline scour and liquefaction have received an increased attention during the last decades, and the modeling and experimental part is well covered especially with respect to 2D scour in non-cohesive soil. Regarding cohesive soil, the experimental part is sparsely investigated, and the modeling part is nearly non-existing. A number of topics are listed below, which need investigations to improve the prediction tool for the pipeline-seabed evaluation.

- *Flow modeling:* Regarding the flow modeling, one improvement needed is to describe the flow with a more accurate Re - variation, thereby reducing scale effects. The combined case of waves and current can still be investigated even more detailed than today, but such investigations most likely do not lead to any deeper fundamental understanding. Obliquely incoming waves and current, potentially with different approach directions, still lacks a throughout analysis. The modeling of the timescale for the scour process can be improved by including the impact of excess turbulence in the wake. This modeling requires an improved turbulence description of the wake, and an improved description of the sediment transport in areas dominated by excess turbulence as demonstrated by Sumer et al. (2003).

- *3D scour development.* This research area is only sparsely covered and restricted to co-directional wave-current motion. Additional investigations are needed in the laboratory and on the modeling side. The numerical modeling tool has been improved during recent years, and work such as Jacobsen (2015) to solve the 3D scour continuity equation is tailor-made for such investigations. Regarding laboratory experiments, the combination of waves and current with different angles of attack needs to be investigated to get an operative realistic model for the span development.

  Nearly all laboratory experiments and models assume the pipe to be straight. One exception is Li et al. (2013), who studied scour near a vertical bend. A special 3D effect also occurs near a horizontal pipeline bend. Such a shift in the horizontal direction is frequently near the inlet to platforms, and sometimes bending more than 90^0. The scour around such a bend may concentrate/diverge the flow, and thus creating 3D scour features, which still awaits investigation.
- *Sediment properties and scour.* The soil properties play a major role in the seabed behavior. Most important is the presence of cohesive sediment, which is difficult to handle experimentally and to model numerically. Regarding non-cohesive sediment, the gradation is very important, because the coarser fractions can armor the bed. None systematic investigations on the impact of the soil gradation on pipeline scour in non-cohesive sediment have been performed for the live bed case.
- *Real environment.* Transforming theoretical and experimental findings to a real environment, where the environmental impact is highly unsteady and 3D with shifting directions of waves and current is a major remaining problem. Draper et al. (2015) made such an attempt regarding the scour behavior during a storm-event, and such investigations should be extended to cover 3D scour effects and liquefaction. The latter shall incorporate history effects.
- *Lateral movement.* Impact of scour on the lateral stability of pipelines needs to be incorporated in existing heuristic models.
- *Natural bed level variations.* While large and small scale bed level variations partly are qualitatively understood, a quantitative description of bank and bar migration is still lacking. Also the interaction

between a pipe and migrating sand waves needs to be investigated with special attention to impact of local seabed curvature and pipeline stiffness.

Notation

a = orbital amplitude;

A = half the soil cross-sectional area displaced by the pipe;

d = mean grain diameter;

D = outer diameter of pipeline;

e = embedment depth of pipe below original seabed;

e_v = void ratio, appearing in Eq. (10);

EI = bending stiffness, appearing in Eq. (9);

$F = U / \sqrt{gD}$ = pipe Froude number;

F_L = hydrodynamic lift force;

g = acc. of gravity;

G = the dimensionless submerged weight of the pipe, defined in Eq. (14);

i = hydraulic gradient;

KC = Keulegan-Carpenter number, defined in Eq. (3);

l_s = stiffness length, Eq. (8);

n = porosity of soil;

p= pressure;

p^+= excess fluid pressure in the sea bed;

Re = Reynolds number, defined in Eq. (5);

1216 s = relative density of sediment;

1217 S_r = relative density of the seabed, defined in Eq. (10);

1218 T = time scale for tunnel erosion;

1219 T^* = non-dimensional time scale, defined in Eq. (7);

1220 U = near-bed flow velocity;

1221 U_c = near bed current velocity;

1222 U_m = maximum orbital velocity at the bed;

1223 W = Submerged weight of fluid-sediment mixture;

1224 W_S = submerged weight of the pipe per unit length;

1225 α_r =relative strength between waves and current defined in Eq. (6);

1226 β = an empirical dimensionless coefficient;

1227 μ = sliding resistance coefficient;

1228 ν = kinematic viscosity of the fluid;

1229 ρ = fluid density;

1230 ρ_p = pipe specific gravity;

1231 ρ_l = specific gravity of the sediment-fluid mixture of liquefied soil;

1232 τ_b = bed shear stress;

1233 θ = The Shields parameter, defined in Eq. (4);

1234

1235

1236 ## References

1237

An, H., Luo, C., Cheng, L. and White, D. (2013). “A new facility for studying ocean-structure–seabed interactions: the O-tube.” *Coastal Eng*., 82, 88–101.

Bernetti, R., Bruschi, R., Valentini, V. and Venturi, M. (1990). “Pipelines placed on erodible Seabeds.” *Proc. 9th Int. Conf. Offshore Mech. and Artic Eng.,* V, 155–164.

Biot, M.A. (1941). “General Theory of Three-Dimensional Consolidation.” *J. Appl. Phys.,*12, 155-164.

Brørs, B. (1999). “ Numerical modelling of flow and scour at pipelines.” *J. Hydraul. Eng.,* 125(5), 511–523.

Chen, B. and Cheng L. (2004). “Numerical investigations of three-dimensional flow and bed shear stress distribution around the span shoulder of pipeline.” *J. Hydrodynamics,* 16(6), 687-694.

Cheng, L. and Chew, L.W. (2003). “Modelling of flow around a near-bed pipeline with a spoiler.” *Ocean Eng.*, 30(13), 1595-1611.

Cheng, L. and Li, F. (2003). “Modeling of local scour below a sagging pipeline.” *Coastal Eng. Journal,* 45(2), 189-210.

Cheng, L., Yeow, K., Zang, Z., Teng, B. (2009). “Three-dimensional scour below pipelines in steady currents.” *Coast. Eng.,* 56(5–6), 577–590.

Cheng, L., Yeow, K., Zang, Z.and Li, F. (2014). “3D scour below pipelines under waves and combined waves and currents.” *Coastal Eng.,* 83, 137–149.

Chiew, Y.M. (1990). “Mechanics of local around submarine pipeline.” *J. Hydraul. Eng.,* 116(4), 515–529.

Chiew, Y.M. (1991a). “Flow Around Horizontal Circular Cylinder in Shallow Flows.” *J. Waterway, Port, Coastal, Ocean Eng.,* 117(2), 120-135.

Chiew, Y.M. (1991b). “Prediction of maximum scour depth at submarine pipelines.” *J. Hydraul. Eng.,* 117(4), 452-466.

Chiew, Y.M. (1992). “Effect of spoilers on scour at submarine pipelines.” *J. Hydraul. Eng.,* 118(9), 1311-1317.

Chiew, Y.M. (1993). “Effect of spoilers on wave-induced scour at submarine pipelines.” *J. Waterway, Port, Coastal, Ocean Eng.,* 119(4), 417-428.

De Grooth, M. B., Bolton, M. D., Foray, P., Meijers, P., Palmer, A. C., Sandven, R., Sawicki, A., and Teh, T.C. (2006). "Physics of Liquefaction Phenomena around Marine Structures." *J. Waterway, Port, Coastal, Ocean Eng.,* 132 (4), 227-243.

Dey, S. and Singh, N.P. (2008). "Clear-Water Scour below Underwater Pipelines under Steady Flow." *J. Hydraul. Eng.,* 134(5), 588-600.

Dey, S., Helkjær, A., Sumer, B.M., and Fredsoe, J. (2011). "Scour at Vertical Piles in Sand-Clay Mixtures under Waves." *J. Waterway, Port, Coastal, Ocean Eng*.137(6), 324-331.

Dogan, M. and Arisoy, Y. (2015). "Scour regime effects on the time scale of wave scour below submerged pipes." *Ocean Eng.,* 104, 673–679.

Drago, M., Mattioli M., Bruschi, R. and Vitali, L. (2015). "Insights on the design of free-spanning pipelines." *Phil. Trans. R. Soc. A* 373 20140112; DOI: 10.1098/rsta.2014.0111.

Draper, S., An, H., Cheng, L. , White, D.J. and Griffiths, T.(2015). "Stability of subsea pipelines during large storms ." *Phil. Trans. R. Soc. A* 373 20140106; DOI: 10.1098/rsta.2014.0106.

Dunn, S.L.,Vun, P.L.,, Chan, A.H. and Damgaard, J.S. (2006). "Numerical Modeling of Wave-Induced Liquefaction around Pipelines." *J. Waterway, Port, Coastal, Ocean Eng.,* 132(4), 276-288.

Elgamal, A., Yang, Z., Parra, E. and Ragheb, A. (2003). "Modeling of cyclic mobility in saturated cohesionless soils." *Int. Journal Plasticity,* (19)6, 883-905.

Foray, P., Bonjean, D. and, Michallet H., and Mory, M. (2006). "Fluid-Soil-Structure Interaction in Liquefaction around a Cyclically Moving Cylinder". *J. Waterway, Port, Coastal, Ocean Eng.,* 132(4), 289-299.

Fredsoe, J. (1978). "Sedimentation of river navigation channels." *J. Hydraul. Div*., 104(2), 223-236.

Fredsoe, J. (1979). "Natural backfilling of pipeline trenches." *J. Petr. Technology,* 31(10), 1223-1230.

Fredsoe, J. and Hansen, E.A. (1987). "Lift forces on pipelines in steady flow." *J. Waterway, Port, Coastal, Ocean Eng.,* 113(2), 139-155.

1283 Fredsoe, J., Hansen, E.A., Mao, Y. and Sumer, B.M. (1988). “Three-dimensional scour below pipelines.” *Trans. ASME , J.*
1284 *Offshore Mech. Arct. Eng.,* 110, 373–379.

1285 Fredsoe, J., Sumer, B.M. and Arnskov, M. (1992). “Time scale for wave/current scour below pipelines.” *Int. J. Offshore*
1286 *and Polar Eng.,* 2(1), 13–17.

1287 Fuhrman, D. R., Baykal, C., Sumer, B.M., Jacobsen, N.G. and Fredsoe, J. (2014). ”Numerical simulation of wave-induced
1288 scour and backfilling processes beneath submarine pipelines.” *Coastal Eng.,* 94, 10-22.

1289 Gao, F-P., Gu, X.Y., Jeng, D.S., Teo, H.T. (2002). ”An experimental study for wave-induced instability of pipelines: the
1290 breakout of pipelines.” *Appl. Ocean Res.,* 24, 83–90.

1291 Gao, F-P., Yang, B., Wu, Y. and Yan, S. (2006). ”Steady current induced seabed scour around a vibrating pipeline.”
1292 *Appl. Ocean Res.,* 28, 291–298.

1293 Gao, F-P., Yan, S., Yang, B. and Wu, Y. (2007). “Ocean currents-induced pipeline lateral stability on sandy seabed.”
1294 *J.Eng. Mech.,* 133(10) 1086-1092.

1295 Gao, F-P. and Luo, C. (2010). “Flow-Pipe-Seepage Coupling Analysis of Spanning Initiation of a Partially-Embedded
1296 Pipeline.” *J. Hydrodynamics, Ser. B,* 22(4), 478–487.

1297 Gao, F-P., Yan, S., Yang, B., and Luo, C. (2011). “Steady flow-induced instability of a partially embedded pipeline: Pipe–
1298 soil interaction mechanism.” *Ocean Eng.,* 38, 934–942.

1299 Gao, F-P., Han,X.T., Cao,J., Sha,Y. and Cui, J.S. (2012). “Submarine pipeline lateral instability on a sloping sandy
1300 seabed.” *Ocean Eng.,* 50, 44-52.

1301 Hale, J.R., Lammert, W.F., Allen, D.W., (1991). “Pipeline on-bottom stability calculations: comparison of two state-of-
1302 the-art methods and pipe–soil model verification.” *Proc. 23rd Ann. Offshore Techn. Conf*., OTC 6761, 567-581.

1303 Hansen, E.A., Staub, C., Fredsoe, J. and Sumer, B.M. (1991). ”Time development of scour induced free spans of
1304 pipelines”. *Proc., 10th Conf. on Offshore Mech. and Arctic Engng. Pipeline Technology,* (V) 25–31.

1305 Hulsbergen, C. H. (1984). “Stimulated self-burial of submarine pipelines.” *Proc. 16th Offshore Tech. Conf.,* OTC 4667,
1306 171-178.

1307 Jacobsen, N.G. (2015). “Mass conservation in computational morphodynamics: uniform sediment and infinite
1308 availability.” *International Journal for Numerical Methods in Fluids,* 78(4), 233-256.

1309 Jacobsen, V., Bryndum, M.B. and Fredsoe, J. (1984). “Determination of Flow Kinematics Close to Marine Pipelines and
1310 Their Use in Stability Calculations.” *Offshore Techn. Conf.*, OTC 4833, 481-49.

1311 Jeng, D.S. (2003). “Wave-induced sea floor dynamics.” *Appl. Mech. Rev*. 56(4), 407-429.

1312 Jeng, D.S. (2013). *Porous Models for Wave-seabed Interactions*, Springer Berlin Heidelberg.

1313 Kazeminezhad, M.H., Yeganeh-Bakhtiary, A., Etemad-Shahidi, A. and Baas, J.H. (2012). ”Two-phase simulation of wave-
1314 induced tunnel scour beneath marine pipelines*.” J. Hydraul.Eng*., 138(6), 517–529.

1315 Kirca, V., Sumer, B., and Fredsoe, J. (2014). ”Influence of Clay Content on Wave-Induced Liquefaction.” *J. Waterway,*
1316 *Port, Coastal, Ocean Eng.*, 140(6), 04014024.
1317 Kiziloz, B., Esin, C. and Yalcin, Y. (2013). “Scour below submarine pipelines under irregular wave attack.” *Coastal*
1318 *Eng.,* 79, 1-8.
1319 Kumar A. V., Neelamani S, and Rao SN. (2003). “Wave pressures and uplift forces on and scour around submarine
1320 pipeline in clayey soil.” *Ocean Eng.,* 30(2), 271–95.
1321 Larsen, B.E., Fuhrman, D.R. and Sumer, B.M. (2016). “Simulation of Wave-Plus-Current Scour beneath Submarine
1322 Pipelines .” *J. Waterway, Port, Coastal, Ocean Eng.*, 04016003.
1323 Leckie, S.H.F., Draper,S. White, D.J., Cheng, L. and Fogliani, A. (2015). ” Lifelong embedment and spanning of a pipeline
1324 on a mobile seabed.” *Coastal Eng.,* 95, 130–146.
1325 Li, F. and Cheng, L., (1999). “A numerical model for local scour under offshore pipelines.” *J. Hydrol. Eng.,* 125(4), 400–
1326 406.
1327 Li, F., Dwivedi, A., Low, Y., Hong, J., and Chiew, Y. (2013). “Experimental Investigation on Scour under a Vibrating
1328 Catenary Riser.” *J.Engng. Mech*., 139(7), 868-878.

1329 Liang, D. and Cheng, L., (2005a). “Numerical modelling of scour below a pipeline in currents. Part I: flow simulation.”
1330 *Coast. Eng.,* 52(1), 25–42.

1331 Liang, D., Cheng, L. and Li, F., (2005b). “Numerical modelling of scour below a pipeline in currents. Part II: scour
1332 simulation.” *Coast. Eng.,* 52(1), 43–62.

1333 Liang, D. and Cheng, L., (2005c). “A numerical model for wave-induced scour below a submarine pipeline.” *J.*
1334 *Waterway, Port, Coastal, Ocean Eng.,* 131(5), 193-202.

1335 Liang, D., Cheng, L. and Yeow, K. (2005d). “Numerical study of the Reynolds-number dependence of two-dimensional
1336 scour beneath offshore pipelines in steady currents.” *Ocean Eng.,* 32(13), 1590-1607.

1337 Liang, D., Cheng, L. and Yeow, K. (2005e). “Numerical model for natural backfill of pipeline trenches subjected to
1338 unidirectional/oscillatory flows.” *China Ocean Eng.,* 19(2), 269-286.

1339 Liu, B. and Jeng, D.S. (2015). “Laboratory Study for Influence of Clay Content (CC) on Wave-Induced Liquefaction in
1340 Marine Sediments.” *Marine Georesources and Geotechnology*, DOI: 10.1080/1064119x.2015.1005322.

1341 Lucassen, R.J. (1984). “Scour underneath submarine pipelines.” *Report No. PL-4 2A. Neth. Mar. Tech. Res. Netherlands*
1342 *Industrial Council for Oceanology*, Delft Univ.Techn.

1343 Mao, Y. (1986). “The interaction between a pipeline and an erodible bed.” PhD thesis, *Series Paper 39, ISVA, Techn.*
1344 *Univ. Denmark*, pp. 178.

1345 Madsen, O.S. (1978). “Wave-induced pore pressures and effective stresses in a poreous bed.” *Geotechnique* 28(4),
1346 377-393.

1347 Mattioli, M., Alsina, J.M., Mancinelli, A., Mozzi, M. and Brocchini, M. (2012). “Experimental investigation of the
1348 nearbed dynamics around a submarine pipeline laying on different types of seabed: The interaction between
1349 turbulent structures and particles.” *Adv. Water Resources,* 48, 31-46.

1350 McDougal, W.G., Tsai, Y.T., Liu, P.L-F. and Clukey, E.C. (1989). “Wave-induced pore-water pressure accumulation in
1351 marine soils.” *J. Offshore Mech. Arctic Eng,*, 111, 1–11.

1352 Mitchener, H., Torfs,H. and Whitehouse,R. (1996). “Erosion of mud/sand mixtures.” *Coastal Eng.*, 29, 1–25.

1353 Miyamoto, J., Sassa, S. and Sekiguchi, H. (2004). “Progressive solidification of a liquefied sand layer during continued
1354 wave loading.” *Geotechnique*, 54(10), 617–629.

1355 Mohr, H., Draper, S. Cheng, L. and White, D.J. (2016). “Predicting the rate of scour beneath subsea pipelines in marine
1356 sediments under steady flow conditions.” *Coastal Eng.* 110, 111–126.

1357 Moshagen, H. and Tørum, A. (1975). “Wave induced pressures in permeable seabeds.” *J. Waterway, Port, Coastal,*
1358 *Ocean Eng.*, 101(1), 49-57.

1359 Myrhaug, D and Rue, H. (2003). “Scour below pipelines and around vertical piles in random waves.” *Coastal Eng.,*
1360 48(4), 227-242.

1361 Oner, A.A. (2010). “The flow around a pipeline with a spoiler.” *Proc. Inst. Mech.Eng. Part C - Journ. Mech. Eng.*
1362 *Science,* 224(C1), 109-121.

1363 Palmer, A.C. and King, R.A. (2004). *Subsea pipeline engineering.* Penwell®.

1364 Postacchini, M. and Brocchini, M. (2015). “Scour depth under pipelines placed on weakly cohesive soils.” *Appl.Ocean*
1365 *Res.* 52, 73–79.

1366 Prevost,J., Andersen, K.H. and Eide, O. (1975). “Discussion of Wave Induced Pressures in Permeable Seabeds.” *J.*
1367 *Waterways Harbors and Coastal Eng. Div.*, 101(4), 464-465.

1368 Rahman, M.S., Booker, J.R. and Seed, H.B. (1977). “Pore Pressure Development under Offshore Gravity Structures.” *J.*
1369 *Geotechn. Eng. Div.,* 103(12), 1419-1436.

1370 Sandven, R., Husby, E., Husby, J., Jønland, J., Roksvåg, K., Stæhli, F., and Tellugen, R. (2007). “Development of a
1371 Sampler for Measurement of Gas Content in Soils.” *J. Waterway, Port, Coastal, Ocean Eng.*, 133(1), 3–13.

1372 Sassa, S. and Sekiguchi, H. (1999). “Wave-induced liquefaction of beds of sand in a
1373 centrifuge.” *Geotechnique*, 49(5), 621–638.

1374 Sawaragi, T. and Deguchi, I. (1992). “Waves on permeable layers.” *Proc. 23rd Int. Conf. Coastal Eng*. ASCE, 1531-1544.

1375 Sawicki, A. (2014). “Mechanics of seabed liquefaction and resolidification.” *Arch. Mech.,* 66(5), 307-328.

1376 Shen, Z.H., Liu Y.B., Li Q.P., Huang Q.H. and Zhu F.R. (2000). “Experiments on interaction between current-induced
1377 vibration and scour of submarine pipelines on sandy bottom.” *China Ocean Engineering,* 14, 423–34.

1378 Sleath, J.F.A. (1970). “Wave-induced pressures in beds of sand.” *Journ. Hydraul. Div.*, 96, 367-378.

1379 Sumer, B.M., Mao, Y. and Fredsoe, J. (1988a). “Interaction between vibrating pipe and erodible bed.” *J. Waterw. Port*
1380 *Coast. Ocean Eng.,* 114(1), 81–92.

1381 Sumer, B., Jensen, H., Mao, Y., and Fredsoe, J. (1988b). “Effect of Lee-Wake on Scour Below Pipelines in Current.” *J.*
1382 *Waterway, Port, Coastal, Ocean Eng.*, 114(5), 599–614.

1383 Sumer, B., Fredsoe, J., Gravesen, H., and Bruschi, R. (1989). “Response of Marine Pipelines in Scour Trenches.” *J.*
1384 *Waterway, Port, Coastal, Ocean Eng.*, 115(4), 477–496.

1385 Sumer, B.M., Fredsoe, J., (1990). “Scour below pipelines in waves.*” J. Waterw. Port Coast. Ocean Eng.* 116(3), 307–
1386 323.

1387 Sumer, B.M. and Fredsoe, J. (1991). “Onset of scour below a pipeline exposed to waves.*” Int. J. Offshore Polar Eng*., 1
1388 (3), 189–194.

1389 Sumer, B.M. and Fredsoe, J. (1994). “Self-burial of Pipelines at Span Shoulders.” *Int. J. Offshore Polar Eng.,* 4(1), 30–
1390 35.

1391 Sumer, B.M. and Fredsoe, J. (1996). “Scour around pipelines in combined waves and current”. *Proc. 7th International*
1392 *Conference on Offshore Mech.Arctic Engng. Conf. Pipeline Techn.,*(V), 595–602.

1393 Sumer, B.M. and Fredsoe, J. (1997). *Hydrodynamics around cylindrical structures.* World Scientific, Singapore.

1394 Sumer, B.M., Fredsoe, J. Christensen,S. and Lind, M.T. (1999). “Sinking/floatation of pipelines and other objects in
1395 liquefied soil under waves.” *Coastal Eng*., 38(2), 53–90.

1396 Sumer, B.M., Truelsen, C., Sichmann, T. and Fredsoe, J. (2001). “Onset of scour below pipelines and self-burial.”
1397 *Coastal Eng.,* 42 (4), 213–235.

1398 Sumer, B.M. and Fredsoe, J. (2002). *The Mechanics of Scour in the Marine Environment*. World Scientific, Singapore.

1399 Sumer, B.M., Chua, L.H.C., Cheng, N.S. and Fredsoe, J. (2003). "Influence of turbulence on bed load sediment
1400 transport." *J.Hydraul. Eng.,* 129(8), 585-596.

1401 Sumer, B.M., Hatipoglu, F., Fredsoe, J. and Sumer, S.K. (2006a). "The sequence of sediment behaviour during wave-
1402 induced liquefaction." *Sedimentology*, 53(3), 611-629.

1403 Sumer, B.M., Truelsen, C. and Fredsoe, J. (2006b). "Liquefaction around pipelines under waves." *J. Waterway, Port,*
1404 *Coastal and Ocean Eng.,* 132(4), 266-275.

1405 Sumer, B.M., Hatipoglu, F., Fredsoe, J. and Hansen, N.E.O. (2006c). "Critical flotation density of pipelines in soils
1406 liquefied by waves and density of liquefied soils." *J. Waterway, Port, Coastal and Ocean Eng.,* 132(4), 252-265.

1407 Sumer, B. M., Hatipoglu, F. and Fredsoe, J. (2007). "Wave scour around a pile in sand, medium dense, and dense silt."
1408 *J. Waterway, Port, Coastal and Ocean Eng.,* 133(1), 14-27.

1409 Sumer, B.M., Dixen, F.H. and Fredsoe, J. (2010*). "*Cover stones on liquefiable soil bed under waves." *Coastal Eng.,* 57
1410 (9), 864-873.

1411 Sumer, B.M. (2014). *Liquefaction around marine structures*, World Scientific , Singapore.

1412 Teh, T. C. , Palmer, A. C. , and Damgaard, J. S. (2003). "Experimental study of marine pipelines on unstable and
1413 liquefied seabed." *Coastal Eng.*, 50, 1–17.
1414 Teh, T.C., Palmer, A.C., Bolton, M.D. and Damgaard, J.S. (2006). "Stability of Submarine Pipelines on Liquefied
1415 Seabeds." *J. Waterway, Port, Coastal, Ocean Eng.,* 132(4), 244-251.

1416 Tian, Y., Cassidy, M.J. and Gaudin, C. (2010). "Advancing pipe–soil interaction models in calcareous sand." *Applied*
1417 *Ocean Research,* (32), 284–297.

1418 Tørum, A. (2007). "Wave-induced pore pressures - Air/gas content." *J. Waterway, Port, Coastal, Ocean Eng.,* 33(1),
1419 83-86.

Van Beek, F.A. and Wind, H.G., (1990). ”Numerical modelling of erosion and sedimentation around offshore pipelines.” *Coastal Eng.*,14(2), 107–128.

Van Rijn, L.C., (1982). “The computation of Bed-load and Suspended Load Transport.” *Report S487-II, Delft Hydraulics Laboratory, Delft.*

Vucetic, M. and Dobry, R. (1991). “Effect of soil plasticity on cyclic response.“ *Journ. Geotechn. Eng., 1*17(1), 89-107.

Wagner, D.A., Murff, J.D., Brennodden, H. and Sveggen, O. (1989). ”Pipe–soil interaction model.” *J. Waterway, Port, Coastal, Ocean Eng.,* 115(2), 205–220.

Westerhorstmann, J.H., Machemehl, J.L., Jo, C.H. (1992). “Effect of pipe spacing on marine pipeline scour.” *Proc. 2nd Int. Offshore And Polar Eng. Conf.,* II, 101-109.

White, D.J. and Cheuk, C.Y. (2008). “Modelling the soil resistance on seabed pipelines during large cycles of lateral movement.” *Mar. struct.,* 21, 59–79.

Wu, Y. and Chiew, Y.M. (2012). “Three-Dimensional Scour at Submarine Pipelines.” *J. Hydraul. Eng.,* 138(9), 788-795.

Wu, Y., and Chiew, Y.M. (2013). “Mechanics of three-dimensional pipeline scour in unidirectional steady current.” *J. Pipeline Systems Eng. and Practice,* 4(1), 3-10.

Wu, Y, and Chiew, Y.M. (2015). “Mechanics of Pipeline Scour Propagation in the Spanwise Direction.” *J. Waterway, Port, Coastal, Ocean Eng.,* 141 (4), Article number 4014045.

Yamamoto, T. (1981). “Wave-induced pore pressures and effective stresses in inhomogeneous seabed foundations.” *Ocean Eng.,* 8(1), 1–16.

Yang, K., Cheng, L., An, H., Bassom, A.P. and Zhao, M. (2013). “The effect of a piggyback cylinder on the flow characteristics in oscillatory flow.” *Ocean Eng.,* 62(1), 45–55.

Yang, L., Shi, B., Guo, Y., Zhang, L., Zhang, J. and Han, Y. (2014). “Scour protection of submarine pipelines using rubber plates underneath the pipes.” *Ocean Eng.,* 84, 176-182.

1442 Zang, Z., Cheng, L., Zhao, M., Liang, D.and Teng, B. (2009). “A numerical model for onset of scour below offshore
1443 pipelines”. *Coastal Eng.,* 56(4), 458–466.

1444 Zang, Z., Cheng, L. and Zhao, M. (2010). “Onset of scour below pipeline under combined waves and current.” *29th Int.*
1445 *Conf. Ocean, Offshore and Arctic Eng,* OMAE2010-20719.

1446 Zhang, J., Stewart, D.P. and Randolph, M.F. (2002). “Kinematic hardening model for pipeline-soil interaction under
1447 various loading conditions.” *Int. Journ. Geomechanics* 2(4), 419–446.

1448 Zhang, Q., Draper S. and Cheng, L. (2016). “Scour below a subsea pipeline in time varying flow conditions.” *Applied*
1449 *Ocean Research* 55, 151–162.

1450 Zhao, M. and Cheng, L. (2008). “Numerical modeling of local scour below a piggyback pipeline in currents.” *J. Hydraul.*
1451 *Eng.,* 134(10), 1452-1463.

1452 Zhao, M. and Cheng, L. (2010). “Numerical investigation of local scour below a vibrating pipeline under
1453 steady currents.” *Coastal Eng.,* 57, 397–406.

1454 Zhao, M., Vaidya , S., Zhang, Q. and Cheng, L. (2015). “Local scour around two pipelines in tandem in steady current.”
1455 *Coastal Eng.,* 98, 1–15.

1456 Zhao, Z. and Fernando, H. J. S. (2008). “Numerical modeling of a sagging pipeline using an Eulerian two-phase model.”
1457 *J. Turbulence,* 9(9), 1-20.

1458 Zhou C, Li G, Dong P, Shi J, and Xu J. (2011). “An experimental study of seabed responses around a marine pipeline
1459 under wave and current conditions.” *Ocean Eng*. 38(1), 226–34.

1460

1461

1462

1463

Figure Caption List

Fig. 1. Vortex system around an embedded pipeline exposed to a current.

Fig. 2. Onset of scour beneath a pipe in current and with waves. Data from Sumer and Fredsoe (1991) and Sumer et al. (2001). Squares: $2 \le KC \le 7$, Circles: $7 \le KC \le 15$, Triangles: $15 \le KC \le 30$. The half-filled symbols include tidal flow next to the waves. Modified from Sumer and Fredsoe (2002)

Fig. 3. Development of the 2D scour profiles with time. The number along the profiles corresponds to evolution in time. Modified from Mao (1986).

Fig. 4. Measured equilibrium depth. Data compiled by Sumer and Fredsoe (1990). Modified from Sumer and Fredsoe (2002).

Fig. 5. Wake system with (a): current and (b): waves. Modified from Sumer and Fredsoe (2002).

Fig. 6. 2D scour in waves. Data by Lucassen (1984) and Sumer and Fredsoe (2002). Modified from Sumer and Fredsoe (2002).

Fig. 7. Experimental data on wave-current tunnel scour. Open symbols from Lucassen (1984): without slash: $3 \le KC \le 7.5$. With left-oriented slash: KC =15, right-orientated: KC = 10. Filled symbols from Sumer and Fredsoe (1996): the numbers in the figure corresponds to their experimental values. Modified from Sumer and Fredsoe (2002).

Fig . 8. Sketch of span shoulders. Modified from Sumer and Fredsoe (2002).

Fig. 9. (A-A): The cycle of embedment at the shoulders. (B-B): Sagging and backfilling in the scour hole. Modified from Sumer and Fredsoe (2002).

1484 **Fig. 10**. Time series of excess pressure at different distances z from the original bed. (Reprinted from

1485 Sumer et al. 2006c, © ASCE).

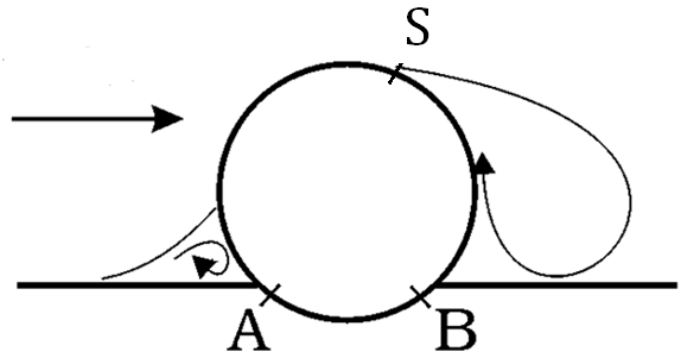

Fig. 1. Vortex system around an embedded pipeline exposed to a current.

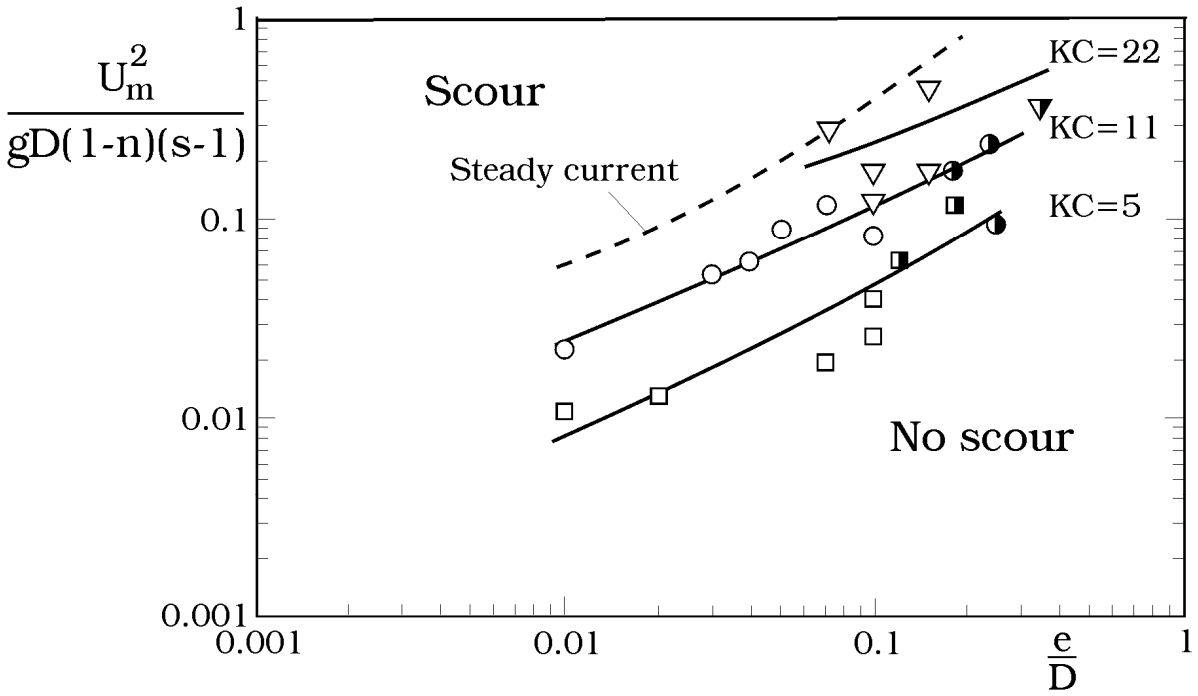

Fig. 2. Onset of scour beneath a pipe in current and with waves. Data from Sumer and Fredsoe (1991) and Sumer et al. (2001). Squares: $2 \le KC \le 7$, Circles: $7 \le KC \le 15$, Triangles: $15 \le KC \le 30$. The half-filled symbols include tidal flow next to the waves. Modified from Sumer and Fredsoe (2002)

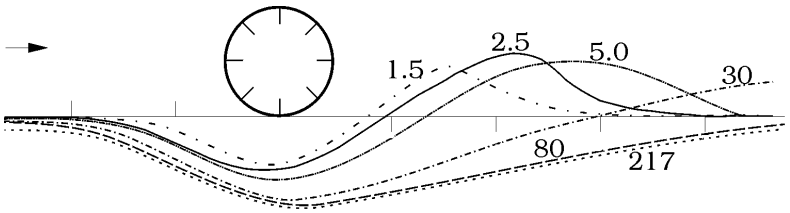

Fig. 3. Development of the 2D scour profiles with time. The number along the profiles corresponds to evolution in time. Modified from Mao (1986).

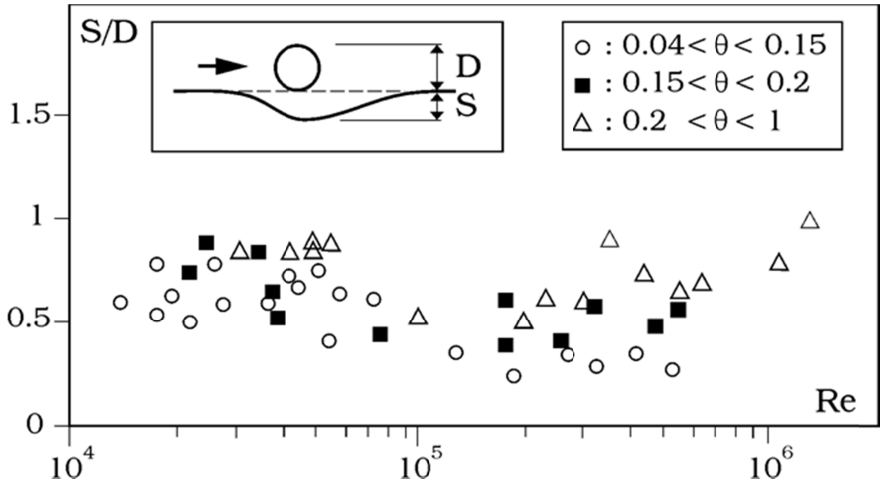

Fig. 4. Measured equilibrium depth. Data compiled by Sumer and Fredsoe (1990). Modified from Sumer and Fredsoe (2002).

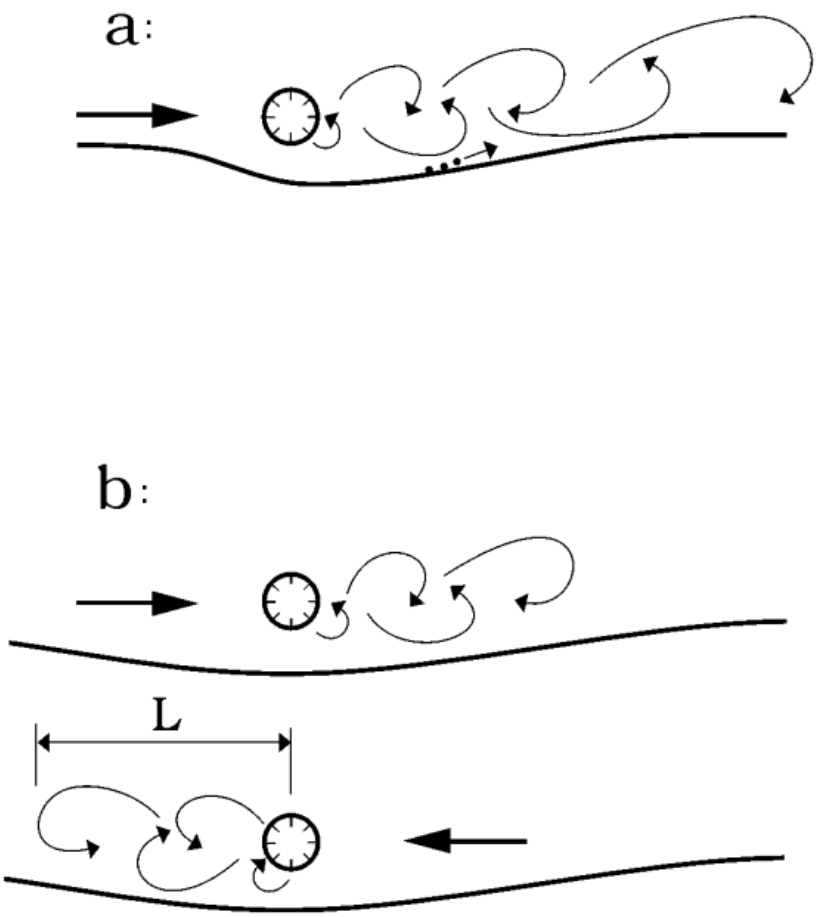

Fig. 5. Wake system with (a): current and (b): waves. Modified from Sumer and Fredsoe (2002).

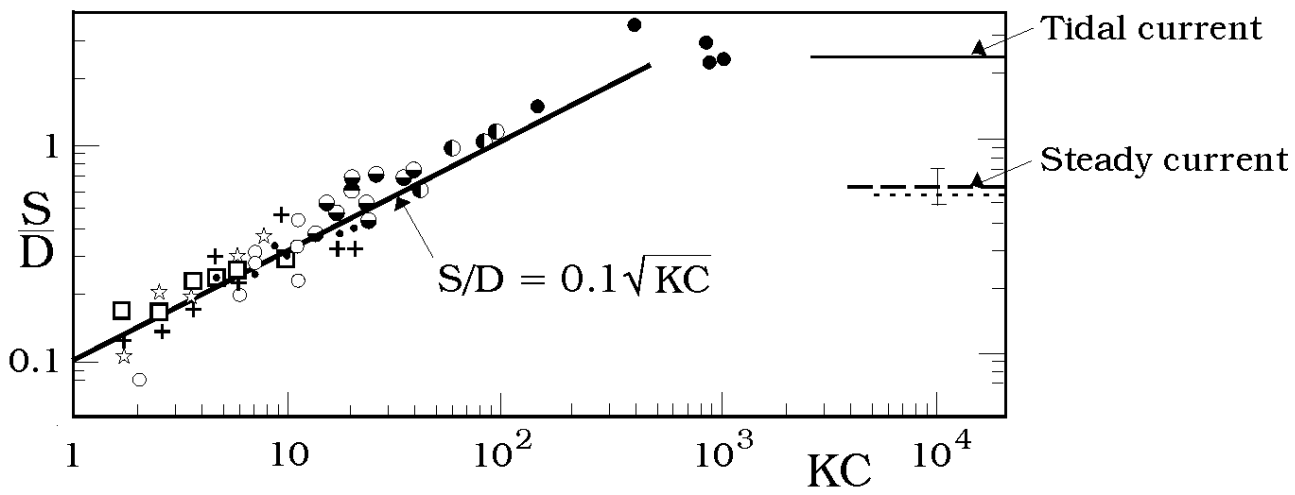

Fig. 6. 2D scour in waves. Data by Lucassen (1984) and Sumer and Fredsoe (2002). Modified from Sumer and Fredsoe (2002).

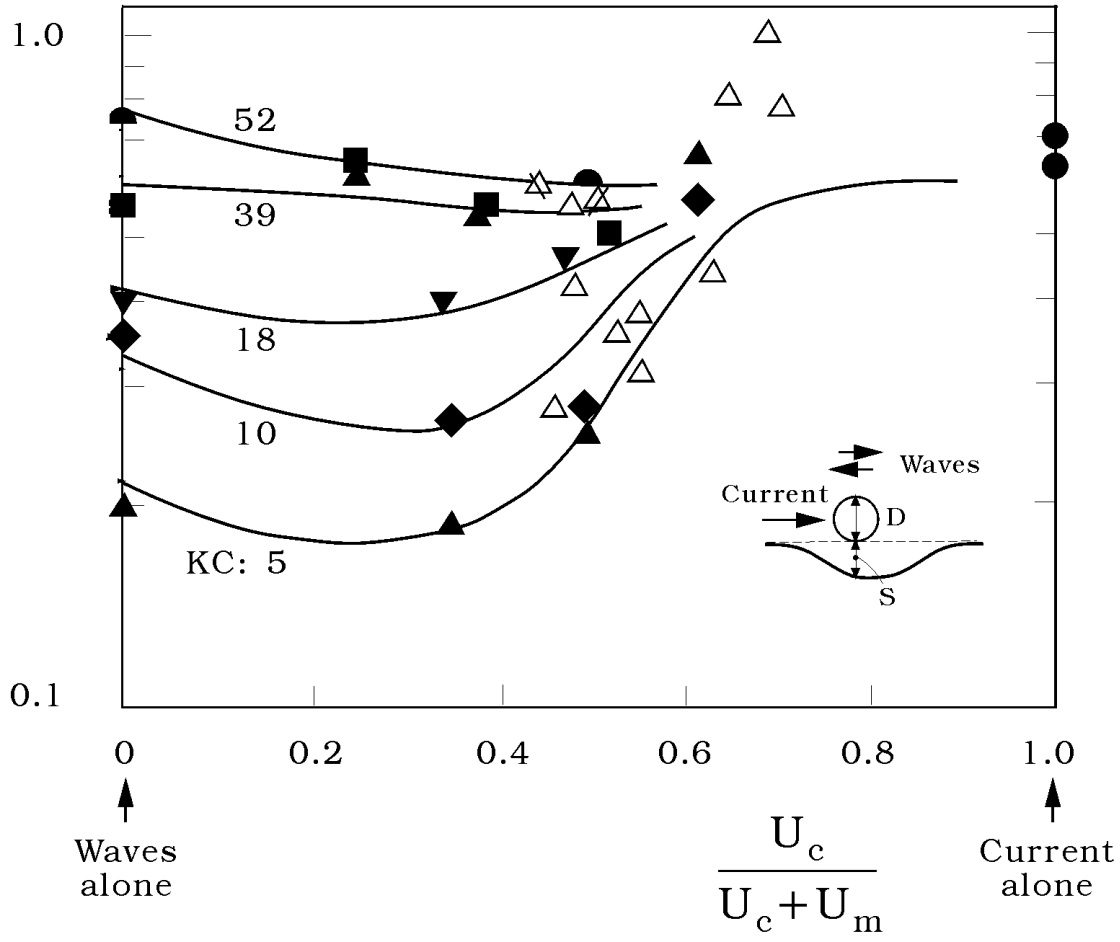

Fig. 7. Experimental data on wave-current tunnel scour. Open symbols: Lucassen (1984). Filled symbols: Sumer and Fredsoe (1996). Lucassen: without slash: $3 \leq KC \leq 7.5$. With left-oriented slash: KC=15, right-orientated: KC= 10. Modified from Sumer and Fredsoe (2002).

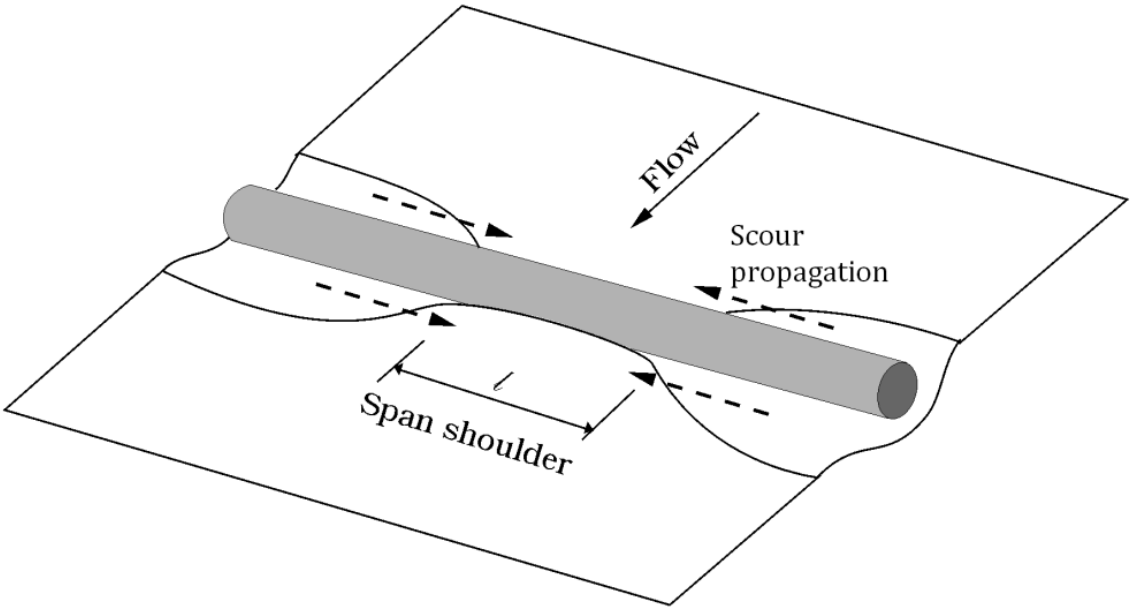

Fig . 8. Sketch of span shoulders. Modified from Sumer and Fredsoe (2002).

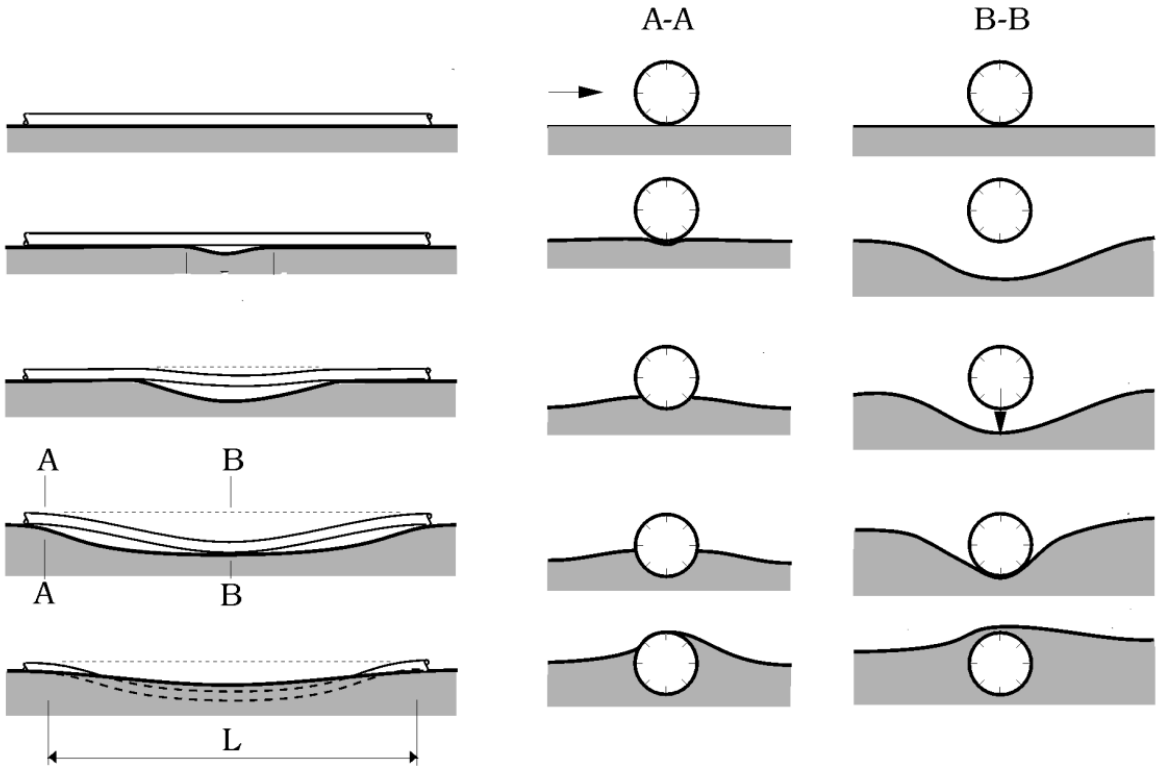

Fig 9. The cycle of embedment at the shoulders (A-A) and sagging and further backfilling in the scour hole (B-B). Modified from Sumer and Fredsoe (2002).

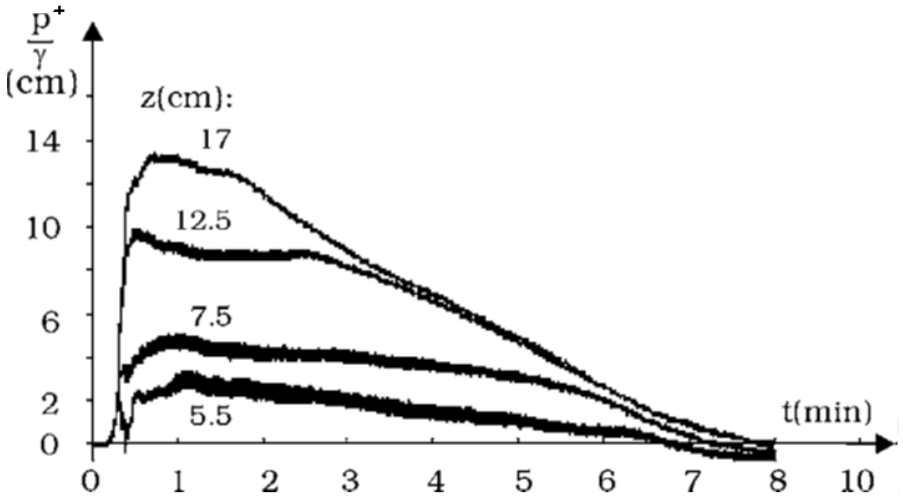

Fig. 10. Time series of excess pressure at different distances z from the original bed. (Reprinted from Sumer et al. 2006c, © ASCE).